(2)

PROBABILISTIC FINITE ELEMENT ANALYSIS

FINAL REPORT

submitted
to the

Office of Naval Research

ONR Grant No. N00014-89-J-1586

submitted
by

Prof. John M. Niedzwecki

Department of Civil Engineering
Texas A & M University
College Station, Texas 77843-3136

February 28, 1992

PROBABILISTIC FINITE ELEMENT ANALYSIS

FINAL REPORT

submitted
to the

Office of Naval Research

ONR Grant No. N00014-89-J-1586

submitted
by

Prof. John M. Niedzwecki

Department of Civil Engineering
Texas A & M University
College Station, Texas 77843-3136

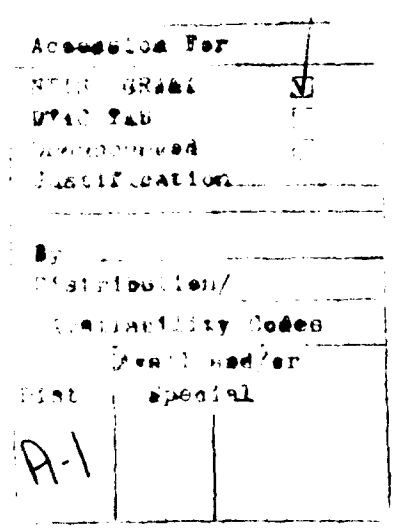

February 28, 1992

Executive Summary

This report contains much of the technical information developed under a research investigation sponsored by ONR Grant N00014-89-J-1586. Additional information on various aspects of this study will continue to appear in the open literature in conference proceeding and forthcoming journal articles.

This research investigation, entitled: *Probabilistic Finite Element Analysis*, focused upon the continued development of recently introduced variational based techniques. Of particular interest was the development of this methodology in the general area of structural mechanics and for ocean related structural problems. The PFE approach holds much promise for complex science and engineering problems since, variabilities in materials and loads can be handled in a very rational manner incorporating probability density functions. Further, the methodology is a computationally efficient alternative to tedious Monte Carlo simulations.

Significant issues presented and addressed as part of this research investigation include: 1.) the definition of appropriate correlation lengths for the PFE model, 2.) the integration of random field concepts, 3.) the development of the methodology to treat significant multi-degree-of- freedom (MDOF) models, 4.) the formulation and computation of second order stress estimates, 5.) the comparison of zeroth order and combined zeroth and second order response estimates for MDOF simulations with Monte Carlo simulations, 6.) the introduction of probability density functions to prescribe both material and load variability, and 7.) the formulation of the force model required to handle long flexible structural members subject to oscillatory flow field kinematics.

An interesting aspect which was demonstrated is that this PFE technology can be incorporated as an add-on to existing finite element software.

PROBABILISTIC FINITE ELEMENT ANALYSIS OF MARINE RISERS

A Thesis

by

H. VERN LEDER

Submitted to the Office of Graduate Studies of
Texas A&M University
in partial fulfillment of the requirements for the degree of

MASTER OF SCIENCE

December 1990

Major Subject: Ocean Engineering

PROBABILISTIC FINITE ELEMENT ANALYSIS OF MARINE RISERS

A Thesis

by

H. VERN LEDER

Approved as to style and content by:

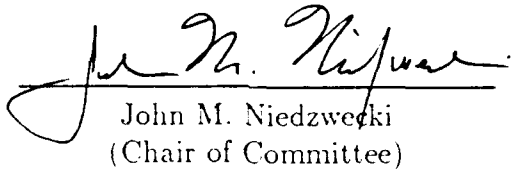

John M. Niedzwecki
(Chair of Committee)

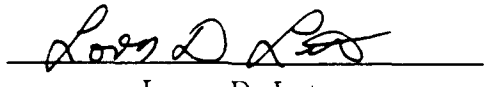

Loren D. Lutes
(Member)

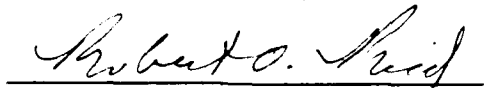

Robert O. Reid
(Member)

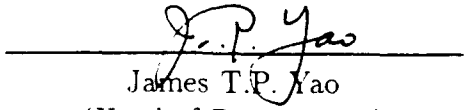

James T.P. Yao
(Head of Department)

December 1990

ABSTRACT

Probabilistic Finite Element Analysis of Marine Risers. (December 1990)

H. Vern Leder, B.S., Texas A&M University;

Chair of Advisory Committee: Dr. J.M. Niedzwecki

The finite element method has been used extensively in structural analyses. Traditionally, the properties of the systems which have been modeled using finite elements have been assumed to be deterministic. The uncertainties in the structural response behavior estimates which result from uncertainties in the properties of the system have been accounted for in design using safety and reduction factors. As structures become more complex and industry makes use of materials such as composites, which are known to have random material properties, an alternative approach to design which quantifies the distributions in response may be required.

Probabilistic finite element techniques, which are capable of assessing the distributions in response behavior for systems with random material properties, loads and boundary conditions are presented in this thesis. One particular method termed second-moment analysis is examined in detail. This method includes perturbation techniques and is used to compute the expected values and covariance matrices of probabilistic response behavior. Second-moment analyses in conjunction with the finite element method require as input the expected values of the random processes inherent to the system and their covariance matrices. Methods are also presented to compute these parameters for local element averages of the random processes which describe the uncertainty in the system.

The offshore industry has assessed the responses and stresses in marine drilling risers using deterministic finite element techniques for many years. This thesis

implements probabilistic finite element techniques as developed in the study to predict the probabilistic response behavior of marine riser systems in which, certain aspects of the problem are considered probabilistic. Specifically, in one set of examples the tension applied to the top of the riser is assumed to be a random variable and in a second set of examples the unit weight of the drilling mud is assumed to vary along the length of the riser. The probabilistic solutions are compared to deterministic solutions for the same riser systems as published by the American Petroleum Institute. Monte Carlo simulations are also performed as a basis of comparison for the probabilistic estimates.

ACKNOWLEDGEMENTS

The author expresses his gratitude to Professor John M. Niedzwecki for his guidance and support. The author also acknowledges Dr. Loren D. Lutes and Professor Robert O. Reid for their valued comments. Appreciation is also expressed to Dr. Rick Mercier and Arun Duggal for their assistance.

This research study was supported by the Office of Naval Research. Contract Number N00014-89-J-1586.

TABLE OF CONTENTS

LIST OF TABLES

LIST OF FIGURES

1 INTRODUCTION

The finite element method provides engineers with the ability to model and obtain computer solutions to complex engineering problems. To date, virtually all structural finite element software packages are formulated within a deterministic framework such that structural material and geometrical properties, damping, loads and boundary conditions are considered in terms of averages, neglecting variations about the average. Since uncertainties are inherent in all phenomena, the effect of variation about the averages is accounted for in design through concepts such as the factor of safety or load factor (Nigam 1983). This approach has proven adequate for many engineering problems where the level of uncertainty is thought to be low. For many other structural problems, however, the degree of randomness is high and the usual deterministic approaches are inadequate for design.

A promising technique which can be used to address these types of problems involves probabilistic methodologies in combination with finite element methods. These require the engineer to identify excessive sources of randomness, construct their probability models, and incorporate the probabilistic distributions into the formulation of the problem (Nigam 1983). Although current finite element software packages do not accommodate this systematic treatment of uncertainty, probabilistic analytical and numerical techniques, consistent with the finite element method, are currently under development. For most complex, probabilistic, structural problems where finite element analysis is required, Monte Carlo simulations and probabilistic, also termed stochastic, finite element methods are suitable. In conjunction with the finite element method, these techniques are used

The following citations follow the style and format of the Journal of Structural Engineering, ASCE.

to assess the probabilistic distributions of structural behavior. They require as input knowledge of the probability distributions of the random parameters inherent to the problem of interest. This includes expected values and variances of random variables and, additionally, correlation functions of random fields. Monte Carlo simulations are fairly straightforward and have been used to solve practical engineering problems, whereas stochastic finite element techniques are a current area of research and only recently, have been developed to the point where they can be used to solve meaningful engineering design problems.

Monte Carlo simulations have been employed in structural analyses where the level of uncertainty was high and a probabilistic distribution of response behavior was required. The technique is suitable for analyses of structures with large displacements, nonlinear material properties and arbitrarily shaped boundaries (Astill 1972). In brief, probabilistic distributions of the sources of randomness are used to generate sample variables or fields which describe the uncertainties; these, in turn, are used as input for the finite element analysis. A distribution of output describing the response behavior is then quantified in terms of statistical parameters. The advantage of Monte Carlo simulation is that no additional formulation to the governing equations of the problem is required. They are, however, computationally repetitive due to the large number of samples of input random variables or fields necessary to achieve statistical stability. In this respect, Monte Carlo simulations are not an entirely attractive approach for estimating complex, probabilistic, structural behavior.

Probabilistic, or stochastic, finite element methods are also applicable techniques for obtaining the probabilistic distributions of structural behavior. These methodologies either formulate probabilistic aspects of the problem directly into the finite element discretization, or incorporate probabilistic formulations into

existing finite element software. As a result, these methods require far less computations than Monte Carlo simulations. Since the techniques are a current area of research, only a limited number of structural problems have been addressed and only at a very fundamental level. Extension of these methodologies, including the numerical techniques involved, is required to develop their full potential. Thus, further research into probabilistic finite element methods is necessary so that a broad range of structural problems can be addressed. Many areas of structural mechanics involve probabilistic aspects. This is particularly true of ocean structures which must routinely operate and survive harsh environmental conditions. Generally, these structures require a dynamic analysis where the degree of uncertainty in many aspects of the problem is high. Stochastic finite element methods provide a numerical technique which quantifies this uncertainty in structural behavior predictions. To date, only Monte Carlo simulations have been used and only to a limited extent in probabilistic offshore–related structural problems.

1.1 Literature Review

At present, development of stochastic finite element analysis methods is a dynamic area of interest in the structural mechanics field. Of particular interest is randomness associated with structural material and geometrical properties as well as stochastic loads, damping and boundary conditions and the overall effects of uncertainty on response estimates. Numerous researchers have contributed to the development of various aspects of stochastic finite element methodologies, and a summary of the more pertinent studies is presented in Table 1. The major thrust of their research has involved characterizing sources of randomness in terms of their probability models and formulating the governing equations of structural

response behavior, consistent with the finite element method, in terms of these distributions.

Many sources of uncertainty inherent to most structures can be modeled as stochastic processes which are functions of space rather than time. These specific processes are the primary focus of stochastic finite element methods. They are generally termed random fields and are explicitly defined in the context of this study as random processes where the random parameter is a function of the spatial coordinates over a structure. In stochastic finite element applications random fields are generally discretized where the discrete values are taken as element averages (Vanmarcke 1984). This requires large correlation distances as compared with element lengths. The techniques employed to characterize these processes as well as other sources of uncertainty found in most structures, as applied to finite element response predictions, are relatively new and therefore the available literature is limited.

Monte Carlo simulations in combination with finite element analyses are one means of obtaining probabilistic solutions to complex, probabilistic, structural problems. Astill, Nossier and Shinozuka (1972) developed a Monte Carlo method capable of assessing structural behavior in problems with spatial variations in material properties. The technique was shown to be completely compatible with the finite element method and thus capable of assessing the effects of irregular boundaries, nonlinear material properties and finite displacements. The authors presented a method to generate digital representations of bivariate random processes from their specified cross-spectral density or equivalent cross-correlation matrix. A large set of conceptual test cylinders with spatially varying modulus and material density were generated in this manner and subjected to an impact load. A finite element analyses was performed on each to determine the stress in

Table 1: Summary of stochastic finite element techniques

STOCHASTIC FINITE ELEMENT TECHNIQUE	APPLICATIONS AS DEMONSTRATED IN THE LITERATURE	REFERENCE
Monte Carlo simulation for structures with spatially varying material properties	Impact loading of an axisymmetric cylinder with stochastic, correlated mass density and ultimate strength	Astill, Nossier and Shinozuka (1972)
Two-dimensional, second moment finite element foundation settlement analyses	Two-dimensional settlement analyses with homogeneous and nonhomogeneous soil profiles and stochastic modulus	Baecher and Ingra (1981)
Second moment analyses for random structures where random fields are uncorrelated with themselves	Dynamic nonlinear truss analysis where members with random yield stress yield	Liu, Belytschko and Mani (1985, 1986)
Transformation of correlated random vector to an uncorrelated random vector via eigenvalue orthogonalization	Second-moment analyses to address elastic/plastic beam and bar with random yield stress and modulus, respectively	Liu, Belytschko and Mani (1987)
Lancoz algorithm to reduce probabilistic finite element equations to smaller sets of equations and removal of secularities	Plane strain continuum with circular hole and random distributed load and modulus	Liu, Besterfield and Belytschko (1988a)
Probabilistic Hu-Washizu variational principle formulation of probabilistic finite element method	Nonlinear elastic response of cantilever beam with random external force, modulus and material properties	Liu, Besterfield and Belytschko (1988b)
Stochastic finite element method utilizing Neumann expansion of operator matrix and consistent Monte Carlo method	None presented	Shinozuka and Dasgupta (1986)
First order expansion of operator matrix where response statistics computed without Monte Carlo simulations	Axial loaded rod with modulus described by random field	Shinozuka and Deodatis (1988)
Representation and analysis of random fields based on the variance function and scale of fluctuation	Deflection of beam with random rigidity described by a random homogeneous field	Vanmarcke and Grigoriu (1983)
Neumann expansion technique used to formulate finite element equations to predict response variability within the framework of the Monte Carlo method	Square finite element mesh with plane-stress square elements constrained on the bottom and uniformly loaded on the top with random modulus	Yamazaki, Shinozuka and Dasgupta (1986)

the cylinder. Useful statistics were extracted from the test results including the mean and standard deviation in stress.

Although the Monte Carlo method is a useful technique for addressing structures with stochastic properties, it is often computationally prohibitive. For example, the ensemble of sample structures must be sufficiently large to accurately describe the random processes in a statistical sense. This requires extensive computer time for both generating the realizations and proceeding with the finite element analyses. Thus, other researchers have attempted to implement the probabilistic aspects of structural analysis directly into the finite element formulation, requiring far less computational effort.

Second–moment analysis, involving perturbation techniques has attracted considerable attention in research involving probabilistic finite element analyses. The method applies to both static and dynamic structural problems where stochastic parameters are described by either random variables or correlated random fields. In short, the second–moment analysis allows for computation of the first–order covariance matrix of structural response, stress, and strain and the expected values of these parameters up to and including second–order. If the random properties are Gaussian, then this method only requires, as input, the first two moments of the random variables or discrete random fields (Yamazaki and Shinozuka 1986). If the relationship between the random parameters inherent to the system and the response behavior is linear, then the method is exact (Ma 1986). For this special case the method is exact for any distribution of the random parameters inherent to the system. In the event that the relationship is nonlinear, the method should prove adequate provided the variances in the random parameters associated with the system are small (Ma 1986). In the case of correlated random fields, the method requires a large correlation distance as compared with element lengths.

The random variables and the discretized stochastic fields are represented by one random vector. The first-order means of structural behavior are obtained using local element averages as input to the finite element analysis. Next, sensitivity vectors are computed by differentiating the parameters of interest with respect to each discrete element of the random vector, where the differentials are evaluated at the mean values of the discrete random elements. For dynamic problems the differentials of the kinematics and stresses can be obtained using implicit time integration techniques which require that the number of time integrations be equal to the dimension of the random vector (Liu, Belytschko and Mani 1985, 1986). In cases involving nonlinear systems or when analytical differentiation of the system matrices is difficult, differentiation of the parameters of interest can be performed using finite difference techniques (Liu, Belytschko and Mani 1985, 1986). At this point, the covariance matrices of the parameters of interest are obtainable. The second-order means, which are estimated from a truncated Taylor series expansion about the mean values of the parameters of interest, are then calculated. If the discrete random fields are uncorrelated, the procedure is simplified. In this case the covariance matrix representing the random vector is a diagonal, thus reducing computational effort (Liu, Belytschko and Mani 1985, 1986). In the second-moment method, the superposition of the covariances of the response for two different, uncorrelated (to each other) random fields of a structure is the same as when both random fields are present simultaneously (Liu, Belytschko and Mani 1987), thus allowing for multiple uncorrelated random fields representing random material properties, loads and boundary conditions.

Second-moment methods consistent with the finite element method have been developed to assess a two-dimensional foundation settlement analysis with a spatially varying modulus of elasticity (Baecher and Ingra 1981). In this problem the

variation about the mean trend of the modulus was treated as one realization of a two-dimensional, second-order stationary random field.

Second-moment analysis techniques have also been used to obtain the probabilistic distributions of dynamic, transient response of truss structures (Liu, Belytschko and Mani 1985, 1986). For problems of this type, consisting of discrete structural elements, the computational procedures are simplified by assuming that the random parameters are uncorrelated. Improved computational procedures have been developed further which enhance the second-moment methodology. To simplify the analysis in problems involving correlated random fields, the full covariance is transformed into a diagonal variance matrix (Liu, Belytschko and Mani 1987). The discretized random vector is, therefore, transformed into an uncorrelated random vector via an eigenvalue orthogonalization procedure. Computations using the second-moment analysis are further reduced due to the fact that only the largest eigenvalues are necessary to represent the random field. It is also possible to discretize the random field using shape functions (Liu, Belytschko and Mani 1987). Further computational efficiency is accomplished by reducing the probabilistic finite element equations to a smaller system of tridiagonal equations using the Lanczos reduction technique (Liu, Besterfield and Belytschko 1988a). This algorithm provides a reduced basis from the system eigenproblem. It also provides a means to eliminate secular terms in higher-order estimates of expected dynamic response parameters, which are known to arise in some specific problems when using second-moment analysis.

A probabilistic Hu-Washizu variational principle formulation has also been used in conjunction with the second-moment analysis to assess probability distributions of response (Liu, Besterfield and Belytschko 1988a). Probabilistic distributions for the compatibility condition, constitutive law, equilibrium, domain

and boundary conditions are incorporated into the variational formulation. Solution of the three stationary conditions for the compatibility relation, constitutive law and equilibrium yield the variations in three fields: displacement; strain and stress. The second–order means and first–order covariance are also computed as above.

Another stochastic finite element method utilizes a Neumann expansion of the operator matrix (Shinozuka and Dasgupta 1986). Again, the random geometrical and material structural properties are represented in terms of a discretized random field with a large correlation distance as compared with element lengths. Unlike second–moment analyses, no partial differentiation is required. The authors first considered the static equation where the response vector was written in terms of a recursive formulation involving the mean response, the inverted mean system stiffness matrix and the deviatoric parts of the corresponding elements in the stiffness matrix. The expected values of displacement, strain and stress vectors of any order and the covariance matrices of these variables can be assessed using this method. A consistent Monte Carlo method was employed to generate the deviatoric stiffness matrices from the normalized fluctuations of the discretized random field about its mean (Shinozuka and Dasgupta 1986). This methodology has also been applied to a prismatic bar with a random modulus subjected to a deterministic static load (Shinozuka and Deodatis 1988). By assuming a power spectrum which described the stochastic field, the covariance matrix of the response displacement vector was calculated analytically as a function of the number of finite elements, thereby eliminating the necessity for Monte Carlo simulations. The method was also used to assess the probabilistic response parameters of a structure with its modulus defined by a two–dimensional random field (Yamazaki, Shinozuka and Dasgupta 1986). In this paper comparisons were

made with Monte Carlo simulations and perturbation techniques.

Further approaches to the development of stochastic finite element methods involved representation of homogeneous random fields in terms of the dimensionless variance function and related scale of fluctuation (Vanmarcke 1984). This approach was formulated for one and two–dimensional random fields. The variance function was shown to measure the "point variance" under local averaging and the scale of fluctuation was defined as the element length times the variance function as the element length approaches infinity. Although these serve as the definitions for the two functions, other interpretations were given, as were models of the variance function for wide–band processes (Vanmarcke 1984). These parameters permit computation of the covariance matrix of "element averages." A shear beam with random rigidity subjected to concentrated and uniformly distributed loads was assessed using this technique (Vanmarcke and Grigoriu 1983).

The procedures mentioned above provide a means for efficient solution of probabilistic structural problems using stochastic finite element analysis. In each method where the random fields are correlated over the structure, the element size is required to be smaller than the maximum length over which appreciable correlation occurs. For problems involving structural dynamics, Monte Carlo methods and second–moment analysis appear to have received the most attention.

1.2 Research Study

Current research into probabilistic finite element methodologies has resulted in computationally efficient techniques which quantify uncertainty in structural problems. The variety of problems considered in the literature is quite limited and, in general, assumptions concerning random structural parameters are required. Research directed at extending and applying the methods to a broader range of

problems would benefit the structural engineer. Of particular interest is the use of probabilistic finite element techniques for offshore applications. Loading scenarios within this environment are stochastic resulting from wind, wave, current and foundation excitation. Uncertainty also exists in the overall damping and force coefficients, necessary for load predictions. Furthermore, material and geometrical uncertainties inherent to structural members also require consideration.

This study focuses on the development and application of stochastic finite element techniques to problems involving offshore structures. A review of the literature indicates that Monte Carlo simulations and second–moment analyses are suitable methods for obtaining the probabilistic distributions of dynamic structural behavior. The second–moment analysis technique is more efficient in terms of computation time, but is untested in offshore related problems. This method, therefore, requires further development where Monte Carlo simulations are useful to provide checks in accuracy.

It is the objective of this thesis study to build upon previous theoretical developments and to implement a stochastic finite element technique which can be directly applied to offshore structural analysis. The stochastic finite element methodology is specifically formulated to address problems involving probabilistic response predictions for an offshore drilling riser. The riser model is described in an American Petroleum Institute (API) bulletin which compares eight industrial riser programs (API 1977). All aspects of the problem in the API bulletin are considered deterministic. For this study, certain parameters in the problem are considered to be probabilistic. One set of examples examines the sensitivity in response behavior to a random pretension applied at the top of the riser. In a second set of examples the unit weight of the drilling mud contained within the riser is assumed to vary along the length of the riser. Probabilistic finite ele-

ment software is developed to estimate the second–order means and first–order variances in responses and stresses. Monte Carlo simulations are also used for comparison of these results. Thus, using probabilistic finite element techniques, a quantitative assessment of uncertainty is achieved. The sensitivity of the overall dynamic response to each of these probabilistic parameters is also obtained. Comparison of probabilistic predictions with those made using deterministic programs developed by industry indicate the relative importance of probabilistic analyses in riser response predictions. It is worth noting that many uncertainties exist in the design and analysis of offshore risers. For this study, only those sources of uncertainty which appear to have the most significant impact on the behavior of the structure are selected for numerical simulations.

2 FORMULATION OF THE SECOND-MOMENT ANALYSIS METHOD

Probabilistic finite element methods involve application of second-moment analysis techniques in conjunction with the finite element method in order to assess the probabilistic distributions of response behavior for stochastic systems. In this chapter the second-moment analysis method is developed in detail and is incorporated into the conventional finite element formulation. The probabilistic finite element method which results is applicable to both static and dynamic problems where the response distributions can be predicted as functions of uncertainties inherent to the system. Sources of randomness include geometrical and material properties, excitation, damping and boundary conditions. Second-moment techniques are exact if a linear relationship exists between the random parameters and the predicted response behavior. If this relationship is moderately nonlinear, then the method should prove adequate for coefficients of variation in the random structural properties less than 0.2 (Ma 1987), where the coefficient of variation is the ratio of standard deviation to the mean. Second-moment analyses require information concerning the distributions of the sources of uncertainty; more specifically the mean and variance for random variables and, additionally, the correlation function for correlated random fields. The correlation distance for random fields is required to be large as compared with the length of discrete elements. Formulation for the probabilistic finite element method incorporating second-moment analysis, as developed by Liu, Belytschko and Mani (1985), is presented below. A probabilistic mass matrix, not addressed by these authors, is also considered.

2.1 Finite Element Equations

Upon completion of a finite element discretization of a structure, the n–degree of freedom equations of motion can be written in matrix form as

$$\boldsymbol{M}\ddot{\boldsymbol{x}}(t) + \boldsymbol{C}\dot{\boldsymbol{x}}(t) + \boldsymbol{K}\boldsymbol{x}(t) = \boldsymbol{F}(t), \tag{1}$$

where $\boldsymbol{M}$, $\boldsymbol{C}$, and $\boldsymbol{K}$ represent the mass, damping and stiffness matrices. The force vector, $\boldsymbol{F}(t)$, and the displacement vector, $\boldsymbol{x}(t)$, are functions of time, t, where the superscript dots represent time derivatives.

If the system matrices and force vector are random functions of uncertainties inherent to the structure, the probabilistic finite element approach may be applicable. Probabilistic distributions of all sources of randomness are incorporated into a q–dimensional random vector, $\boldsymbol{b}$, such that the equation of motion now can be expressed as

$$\boldsymbol{M}(\boldsymbol{b})\ddot{\boldsymbol{x}}(\boldsymbol{b},t) + \boldsymbol{C}(\boldsymbol{b})\dot{\boldsymbol{x}}(\boldsymbol{b},t) + \boldsymbol{K}(\boldsymbol{b})\boldsymbol{x}(\boldsymbol{b},t) = \boldsymbol{F}(\boldsymbol{b},t). \tag{2}$$

2.2 Random Vector Formulation

Formulation of the random vector can be visualized by considering Figure 1. In Figure 1a the beam, whose thickness is a homogeneous random function of the axial coordinate, is subject to a harmonic point load with a random amplitude. The process corresponding to the beam thickness, $a(z)$ is shown in Figure 1b, where the mean trend is specified as $\mathrm{E}[a(z)]$. If the mean trend is extracted from the process corresponding to the beam thickness, then the constant variance is denoted $\mathrm{var}[a]$ and the correlation of $a(z)$ is represented by the function $\rho_a(\tau)$, where τ is an arbitrary correlation length. The distribution of the random force

amplitude, A, is specified in terms of its mean, E[A], and its variance, var[A].

Once all of the significant sources of randomness and their probability models have been identified, the random vector, $\boldsymbol{b}$, can be formulated. The elements of $\boldsymbol{b}$ represent correlated distributions of local spatial averages of stochastic properties (i.e., beam thickness), or distributions of random variables (i.e., force amplitude). From Figure 1c, the beam is discretized into n elements where the length of element $\imath$ is $\ell_\imath$. The process representing the beam thickness is then averaged over each element such that the variable, $a_\imath$ represents the distribution of the average of $a(z)$ over element $\imath$. If the process is assumed to be ergodic in the mean, the expected value of $a_\imath$ is equal to E[$a(z)$].

For this example the dimension of the random vector becomes $(n+1)$, where the first n elements of $\boldsymbol{b}$ represent correlated discrete distributions of the mean beam thickness over elements $(1,\ldots,n)$ and the $(n+1)$th element of $\boldsymbol{b}$ represents the distribution of the force amplitude. Thus, $\boldsymbol{b}$ is equal to $(b_1,\ldots,b_n,b_{n+1})$ and represents the distributions of $(a_1,\ldots,a_n,A)$.

The vector, $\bar{\boldsymbol{b}}$, is defined as a mean vector where each element of $\bar{\boldsymbol{b}}$ represents the expected value of the corresponding element in the random vector (i.e., $\bar{b}_\imath$ = E[$b_\imath$]). A probabilistic analysis requires, in addition to $\bar{\boldsymbol{b}}$, the covariance between the elements of $b_\imath$ and $b_\jmath$. Since the random field, $a(z)$, is correlated with itself and uncorrelated to the harmonic excitation amplitude, the covariance matrix, Cov[$b_\imath, b_\jmath$], becomes

$$\mathrm{Cov}[b_\imath, b_\jmath] = \begin{cases} \mathrm{Cov}[a_\imath, a_\jmath] & \text{if } \imath \le n, \jmath \le n \\ \mathrm{var}[A] & \text{if } \imath = \jmath = n+1 \\ 0 & \text{otherwise} \end{cases} . \tag{3}$$

1a.

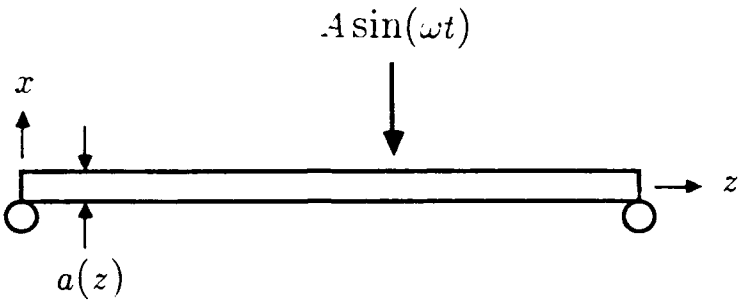

1b.

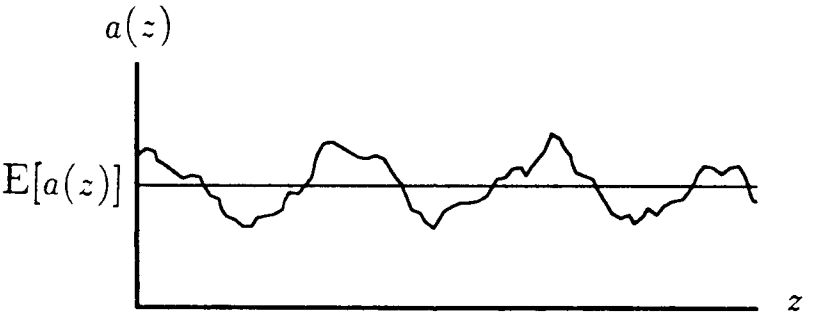

1c.

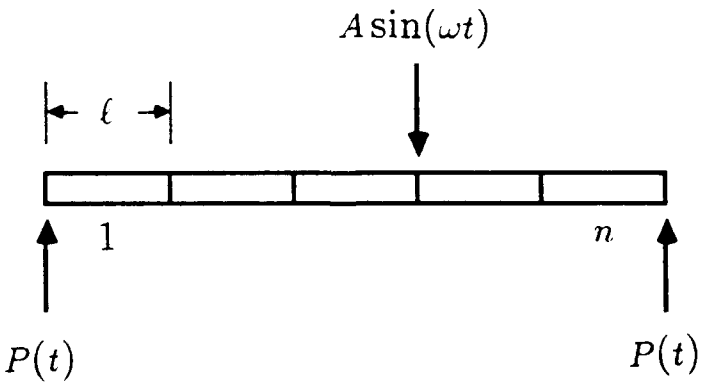

Figure 1: Beam with stochastic properties.

2.3 The Correlation Function

Intuitively, as an element length shown in Figure 1c approaches zero, the variance in the local spatially averaged process, var$[a_i]$, approaches the variance of the entire process, and as ℓ_i becomes large var$[a_i]$ approaches zero for an ergodic in the mean process. Vanmarcke and Grigoriu (1983) propose a technique by which the covariance function of discretized one–dimensional random fields may be computed as a function of element lengths and position. Consider Figure 2 which depicts the same random field as in the previous example. Assuming $a(z)$ has been averaged over the same arbitrary element lengths as before, the covariance between a_1 and a_n can be expressed as follows

$$\text{Cov}[a_1, a_n] = \frac{\text{var}[a]}{2\ell_1\ell_n}\left[Z_0^2\gamma_a(Z_0) - Z_1^2\gamma_a(Z_1) + Z_2^2\gamma_a(Z_2) - Z_3^2\gamma_a(Z_3)\right], \quad (4)$$

where $\gamma_a(Z_i)$ is the variance function which depicts the dependence of the variance of spatial averages on the size of the averaging interval, Z_i (Vanmarcke and Grigoriu 1983). The covariances between any of the element averages, a_i and a_j, can be computed in similar fashion upon substitution of a_i, a_j, ℓ_i and ℓ_j for a_1, a_n, ℓ_1 and ℓ_n and consistently defining Z_0, Z_1, Z_2 and Z_3 as depicted in Figure 2. The variance function is a ratio of the variance of the spatially averaged process to the variance of the entire process and is computed as

$$\gamma_a(Z) = \frac{2}{Z}\int_0^Z \left(1 - \frac{\tau}{Z}\right)\rho_a(\tau)\,d\tau. \quad (5)$$

The variance in a_i can also be computed from the variance function

$$\text{var}[a_i] = \text{var}[a]\gamma_a(\ell_i). \quad (6)$$

Use of the exact variance function in conjunction with Equation 4 yields exact

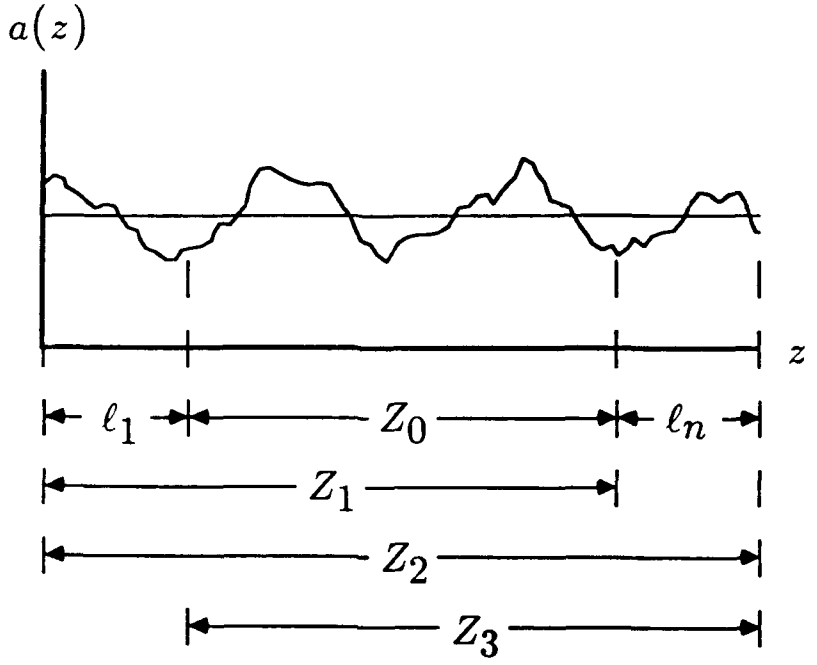

Figure 2: Definition of distances in expression for covariances between spatial averages.

results for the covariances of element properties (Vanmarcke and Grigoriu 1983). Unfortunately, adequate information concerning the correlation function is seldom available to the analyst. Vanmarcke (1983) has proposed approximate expressions for the variance function which are exact for many wide band processes so that a detailed description of the correlation function is not required. The methodology has also been extended to two-dimensional random fields (Vanmarcke 1983).

It should be noted that as the element lengths are increased, the sampling variability is reduced and important information may be lost. Thus, the correlation length, L_c, which represents the maximum correlation distance over which appreciable correlation occurs, is required to be large as compared with the lengths of the elements. Several probabilistic finite element studies have examined the sensitivity of probabilistic response estimates to the correlation length (Baecher and Ingra 1981, Shinozuka and Deodatis 1988, etc.)

2.4 Random Field Discretization

An alternative approach to the random vector discretization involves the use of interpolation functions to approximate the random field (Liu, Belytschko and Mani 1987). The method can be used to predict the expected value and the covariance functions for a continuous random field provided the expected value and covariance function for discrete values of the random field are known. Consider the case of a beam where the thickness, $a(z)$, varies along the axial coordinate, z. If the process is discretized such that a discrete value of the beam thickness is denoted as a_i, where $i = 1, \ldots, q$, then the beam thickness can be approximated at any point using the discretization

$$a(z) = \sum_{i=1}^{q} \phi_i(z) a_i, \tag{7}$$

where $\phi_i(z)$ represents the individual shape functions, which are independent of those used in the finite element discretization. It follows that the expected value of $a(z)$ is approximated as

$$\begin{aligned} \mathrm{E}[a(z)] &= \int_{-\infty}^{+\infty} a(z)\mathrm{p}(a)\, da \\ &= \sum_{i=1}^{q} \phi_i(z)\mathrm{E}[a_i], \end{aligned} \tag{8}$$

where $\mathrm{p}(a)$ is the probability density function of a. The covariance between any two points of the continuous process, $a(z_l)$ and $a(z_m)$, can be approximated as

$$\begin{aligned} \mathrm{Cov}[a(z_l), a(z_m)] &= \int_{-\infty}^{+\infty} (a(z_l) - \mathrm{E}[a(z_l)])(a(z_m) - \mathrm{E}[a(z_m)])\mathrm{p}(a)\, da \\ &= \sum_{i=1}^{q}\sum_{j=1}^{q} \{\phi_i(z_l)\phi_j(z_m)\mathrm{Cov}[a_i, a_j]\}\,. \end{aligned} \tag{9}$$

Note that each discrete value of the beam thickness represents an individual element in the random vector, $\boldsymbol{b}$. Thus, elements which are large, as compared with the length of the random field discretization, will contribute a large number of components to the random vector. There is no obvious advantage to including each discrete point in the process when developing the random vector, as opposed to using the technique proposed by Vanmarcke, where only the local spatial averages over the individual elements are considered. In this study, the local spatial averaging techniques, as suggested by Vanmarcke, are used to develop the random vector.

2.5 Taylor Series Expansion

Application of second–moment analysis in the development of probabilistic finite element methods involves expanding all random functions about the mean value of each element of $\boldsymbol{b}$ via a Taylor series expansion and retaining up to and including second–order terms. For a small parameter, γ , the discrete random displacement vector, $\boldsymbol{x}(\boldsymbol{b},t)$, is expanded about $\bar{\boldsymbol{b}}$ via a second–order perturbation as follows

$$\boldsymbol{x}(\boldsymbol{b},t) = \bar{\boldsymbol{x}}(t) + \gamma \sum_{i=1}^{q} \left\{ \left. \frac{\partial \boldsymbol{x}(t)}{\partial b_i} \right|_{\bar{\boldsymbol{b}}} \Delta b_i \right\} + \frac{1}{2}\gamma^2 \sum_{i=1}^{q}\sum_{j=1}^{q} \left\{ \left. \frac{\partial^2 \boldsymbol{x}(t)}{\partial b_i \partial b_j} \right|_{\bar{\boldsymbol{b}}} \Delta b_i \Delta b_j \right\}, \quad (10)$$

where the vector $\bar{\boldsymbol{x}}(t)$ is the zeroeth–order displacement given by $\boldsymbol{x}(\bar{\boldsymbol{b}},t)$. The partial derivatives $\frac{\partial \boldsymbol{x}(t)}{\partial b_i}$ and $\frac{\partial^2 \boldsymbol{x}(t)}{\partial b_i \partial b_j}$ are evaluated at $\bar{\boldsymbol{b}}$ and represent the first–order variation of displacement with respect to b_i and the second–order variation of displacement with respect to b_i and b_j, respectively. The variable Δb_i represents the first–order variation of b_i about $\mathrm{E}[b_i]$. Similar expressions can be developed for velocity and acceleration vectors by taking first and second–order time derivatives of Equation 10. The mass, stiffness and damping matrices and the stochastic force vector can also be obtained using second–order perturbation techniques

$$\boldsymbol{M}(\boldsymbol{b}) = \bar{\boldsymbol{M}} + \gamma \sum_{i=1}^{q} \left\{ \left. \frac{\partial \boldsymbol{M}}{\partial b_i} \right|_{\bar{\boldsymbol{b}}} \Delta b_i \right\} + \frac{1}{2}\gamma^2 \sum_{i=1}^{q}\sum_{j=1}^{q} \left\{ \left. \frac{\partial^2 \boldsymbol{M}}{\partial b_i \partial b_j} \right|_{\bar{\boldsymbol{b}}} \Delta b_i \Delta b_j \right\}, \quad (11)$$

$$\boldsymbol{C}(\boldsymbol{b}) = \bar{\boldsymbol{C}} + \gamma \sum_{i=1}^{q} \left\{ \left. \frac{\partial \boldsymbol{C}}{\partial b_i} \right|_{\bar{\boldsymbol{b}}} \Delta b_i \right\} + \frac{1}{2}\gamma^2 \sum_{i=1}^{q}\sum_{j=1}^{q} \left\{ \left. \frac{\partial^2 \boldsymbol{C}}{\partial b_i \partial b_j} \right|_{\bar{\boldsymbol{b}}} \Delta b_i \Delta b_j \right\}, \quad (12)$$

$$\boldsymbol{K}(\boldsymbol{b}) = \bar{\boldsymbol{K}} + \gamma \sum_{i=1}^{q} \left\{ \left. \frac{\partial \boldsymbol{K}}{\partial b_i} \right|_{\bar{\boldsymbol{b}}} \Delta b_i \right\} + \frac{1}{2}\gamma^2 \sum_{i=1}^{q}\sum_{j=1}^{q} \left\{ \left. \frac{\partial^2 \boldsymbol{K}}{\partial b_i \partial b_j} \right|_{\bar{\boldsymbol{b}}} \Delta b_i \Delta b_j \right\}, \quad (13)$$

$$\boldsymbol{F}(\boldsymbol{b},t) = \bar{\boldsymbol{F}}(t) + \gamma \sum_{i=1}^{q} \left\{ \left. \frac{\partial \boldsymbol{F}(t)}{\partial b_i} \right|_{\bar{\boldsymbol{b}}} \Delta b_i \right\} + \frac{1}{2}\gamma^2 \sum_{i=1}^{q}\sum_{j=1}^{q} \left\{ \left. \frac{\partial^2 \boldsymbol{F}(t)}{\partial b_i \partial b_j} \right|_{\bar{\boldsymbol{b}}} \Delta b_i \Delta b_j \right\}. \quad (14)$$

The matrix functions $\bar{\boldsymbol{M}}$, $\bar{\boldsymbol{C}}$, $\bar{\boldsymbol{K}}$ and $\bar{\boldsymbol{F}}(t)$ represent the mass, damping and stiffness matrices and the external force vector evaluated at $\bar{\boldsymbol{b}}$. The first–order derivatives represent first–order variations in the matrix functions with respect to b_i and they indicate the sensitivity of the functions to fluctuations about the mean value of random properties inherent to the system. The second–order differentials represent second–order variations in the matrix functions with respect to b_i and b_j and they indicate the sensitivity of the first–order derivatives to fluctuations about the mean values of the random properties.

The mass, damping and stiffness matrices and the external force vector are generally represented using analytical expressions, thus allowing the required differentiation. For certain nonlinear systems where analytical differentiation is not possible, the governing equations can be differentiated using finite difference techniques such as the central difference method (Liu, Belytschko & Mani 1985). Introducing Equations 10–14 into Equation 2 and segregating the resulting equation into terms of order 1, γ and γ^2 yields three independent equations. These include zeroeth-, first-, and second–order equations which are used to evaluate $\bar{\boldsymbol{x}}(t)$, $\frac{\partial \boldsymbol{x}(t)}{\partial b_i}$ and $\frac{\partial^2 \boldsymbol{x}(t)}{\partial b_i \partial b_j}$ at $\bar{\boldsymbol{b}}$. These vectors are in turn utilized to determine the distribution of response at any time, t.

2.6 Zeroeth–Order Equation

The zeroeth–order equation is assessed by evaluating Equation 2 at the mean value of all sources of randomness inherent to the system, and thus is analogous to the deterministic approach where all deviations about the mean are ignored. The zeroeth–order equation is expressed as

$$\bar{\boldsymbol{M}}\ddot{\bar{\boldsymbol{x}}}(t) + \bar{\boldsymbol{C}}\dot{\bar{\boldsymbol{x}}}(t) + \bar{\boldsymbol{K}}\bar{\boldsymbol{x}}(t) = \bar{\boldsymbol{F}}(t). \tag{15}$$

Solutions for the kinematics are obtained using a numerical time integration technique such as the implicit Newmark method (Bathe 1982).

2.7 First–Order Equations

To obtain the first–order equations of motion, Equation 2 is differentiated with respect to each element of the random vector. Thus, the sensitivity in the kinematics to b_i are computed from the following first–order equation

$$\bar{M}\left.\frac{\partial \ddot{\boldsymbol{x}}(t)}{\partial b_i}\right|_{\bar{\boldsymbol{b}}} + \bar{C}\left.\frac{\partial \dot{\boldsymbol{x}}(t)}{\partial b_i}\right|_{\bar{\boldsymbol{b}}} + \bar{K}\left.\frac{\partial \boldsymbol{x}(t)}{\partial b_i}\right|_{\bar{\boldsymbol{b}}} =$$

$$\left.\frac{\partial \boldsymbol{F}(t)}{\partial b_i}\right|_{\bar{\boldsymbol{b}}} - \left[\left.\frac{\partial \boldsymbol{M}}{\partial b_i}\right|_{\bar{\boldsymbol{b}}} \ddot{\bar{\boldsymbol{x}}}(t) + \left.\frac{\partial \boldsymbol{C}}{\partial b_i}\right|_{\bar{\boldsymbol{b}}} \dot{\bar{\boldsymbol{x}}}(t) + \left.\frac{\partial \boldsymbol{K}}{\partial b_i}\right|_{\bar{\boldsymbol{b}}} \bar{\boldsymbol{x}}(t)\right]. \tag{16}$$

The sensitivity vectors, $\left.\frac{\partial \boldsymbol{x}(t)}{\partial b_i}\right|_{\bar{\boldsymbol{b}}}$, $\left.\frac{\partial \dot{\boldsymbol{x}}(t)}{\partial b_i}\right|_{\bar{\boldsymbol{b}}}$ and $\left.\frac{\partial \ddot{\boldsymbol{x}}(t)}{\partial b_i}\right|_{\bar{\boldsymbol{b}}}$, are computed using the same numerical time integration technique as employed to solve the zeroeth–order equation. Note that the total number of first-order equations to be solved is equal to the dimension of the random vector.

2.8 Second–Order Equation

The second–order equation is assessed to obtain second–order deviations about the mean response, $\Delta\bar{\boldsymbol{x}}(t)$, and is computed from the following equation

$$\bar{M}\Delta\ddot{\bar{\boldsymbol{x}}}(t) + \bar{C}\Delta\dot{\bar{\boldsymbol{x}}}(t) + \bar{K}\Delta\bar{\boldsymbol{x}}(t) = \Delta\hat{\boldsymbol{F}}(t), \tag{17}$$

where

$$\Delta\hat{\boldsymbol{F}}(t) = \frac{1}{2}\sum_{i=1}^{q}\sum_{j=1}^{q}\left\{\left.\frac{\partial^2\boldsymbol{F}(t)}{\partial b_i \partial b_j}\right|_{\bar{\boldsymbol{b}}} \mathrm{Cov}[b_i, b_j]\right\}$$

$$-\sum_{i=1}^{q}\sum_{j=1}^{q}\left\{\left[\left.\frac{\partial \boldsymbol{M}}{\partial b_i}\right|_{\bar{\boldsymbol{b}}}\left.\frac{\partial \ddot{\boldsymbol{x}}(t)}{\partial b_j}\right|_{\bar{\boldsymbol{b}}} + \left.\frac{\partial \boldsymbol{C}}{\partial b_i}\right|_{\bar{\boldsymbol{b}}}\left.\frac{\partial \dot{\boldsymbol{x}}(t)}{\partial b_j}\right|_{\bar{\boldsymbol{b}}} + \left.\frac{\partial \boldsymbol{K}}{\partial b_i}\right|_{\bar{\boldsymbol{b}}}\left.\frac{\partial \boldsymbol{x}(t)}{\partial b_j}\right|_{\bar{\boldsymbol{b}}}\right]\mathrm{Cov}[b_i, b_j]\right\}$$

$$-\frac{1}{2}\sum_{i=1}^{q}\sum_{j=1}^{q}\left\{\left[\left.\frac{\partial^2 \boldsymbol{M}}{\partial b_i \partial b_j}\right|_{\bar{\boldsymbol{b}}}\ddot{\bar{\boldsymbol{x}}}(t) + \left.\frac{\partial^2 \boldsymbol{C}}{\partial b_i \partial b_j}\right|_{\bar{\boldsymbol{b}}}\dot{\bar{\boldsymbol{x}}}(t) + \left.\frac{\partial^2 \boldsymbol{K}}{\partial b_i \partial b_j}\right|_{\bar{\boldsymbol{b}}}\bar{\boldsymbol{x}}(t)\right]\mathrm{Cov}[b_i, b_j]\right\}, \quad (18)$$

and $\Delta\bar{\boldsymbol{x}}(t)$ can be written as

$$\Delta\bar{\boldsymbol{x}}(t) = \frac{1}{2}\sum_{i=1}^{q}\sum_{j=1}^{q}\left\{\left.\frac{\partial^2 \boldsymbol{x}(t)}{\partial b_i \partial b_j}\right|_{\bar{\boldsymbol{b}}}\mathrm{Cov}[b_i, b_j]\right\}. \quad (19)$$

Upon substitution of the zeroeth–order kinematics, sensitivity vectors and second–order differentials of the system matrices and force vector, all evaluated at $\bar{\boldsymbol{b}}$, into Equation 18, the second–order equation of motion, Equation 17, can be computed in terms of $\Delta\bar{\boldsymbol{x}}(t)$, $\Delta\dot{\bar{\boldsymbol{x}}}(t)$ and $\Delta\ddot{\bar{\boldsymbol{x}}}(t)$ using the same numerical time integration scheme.

2.9 Probability Distributions of Response Estimates

After solutions to Equations 15–17 have been obtained, the expected value of the response kinematics accurate to second–order and the covariance between elements l and m of the response kinematic vectors can be ascertained. As defined in Ma (1987), the second–order accurate expected value of an arbitrary random vector, $\boldsymbol{g}(\boldsymbol{b})$, is

$$\mathrm{E}[\boldsymbol{g}(\boldsymbol{b})] \approx \bar{\boldsymbol{g}} + \frac{1}{2}\sum_{i=1}^{q}\sum_{j=1}^{q}\left\{\left.\frac{\partial^2 \boldsymbol{g}}{\partial b_i \partial b_j}\right|_{\bar{\boldsymbol{b}}}\mathrm{Cov}[b_i, b_j]\right\}. \quad (20)$$

Thus, the second–order response vector at time, t, can now be defined as

$$\mathrm{E}[\boldsymbol{x}(\boldsymbol{b},t)] \approx \bar{\boldsymbol{x}}(t) + \Delta\bar{\boldsymbol{x}}(t). \tag{21}$$

The $n \times n$ covariance matrix for the response at degree of freedoms l and m is computed from the following first-order formula (Liu Belytschko and Mani 1987)

$$\mathrm{Cov}[x_l(t), x_m(t)] \approx \sum_{i=1}^{q}\sum_{j=i}^{q}\left\{\left(\frac{\partial x_l(t)}{\partial b_i}\bigg|_{\bar{\boldsymbol{b}}}\right)\left(\frac{\partial x_m(t)}{\partial b_j}\bigg|_{\bar{\boldsymbol{b}}}\right)\mathrm{Cov}[b_i, b_j]\right\}. \tag{22}$$

The variance in response at degree of freedom l is thus defined as

$$\mathrm{var}[x_l(t)] \approx \sum_{i=1}^{q}\sum_{j=1}^{q}\left\{\left(\frac{\partial x_l(t)}{\partial b_i}\bigg|_{\bar{\boldsymbol{b}}}\right)\left(\frac{\partial x_l(t)}{\partial b_j}\bigg|_{\bar{\boldsymbol{b}}}\right)\mathrm{Cov}[b_i, b_j]\right\}. \tag{23}$$

Note that the second-order accurate expected values in structural velocities and accelerations and their first-order accurate covariance matrices can also be computed by taking the appropriate time derivatives of Equations 21 and 22.

2.10 Computational Aspects of the Probabilistic Finite Element Method

The computational aspects of the probabilistic finite element method are presented in a flowchart in Figure 3. The amount of computation time required by the analysis is reduced if the covariance matrix, $\mathrm{Cov}[b_i, b_j]$ is not full, as in the case of uncorrelated elements in $\boldsymbol{b}$. For example, when no correlation exists between any of the elements of $\boldsymbol{b}$, Equation 22 reduces to

$$\mathrm{var}[x_l(t)] \approx \sum_{i=1}^{q}\left\{\left(\frac{\partial x_l(t)}{\partial b_i}\bigg|_{\bar{\boldsymbol{b}}}\right)^2 \mathrm{var}[b_i]\right\}. \tag{24}$$

When the correlation between a number of elements of $\boldsymbol{b}$ is high, the covariance matrix can be reduced to a diagonal to enhance computational efficiency. This is accomplished via an eigenvalue orthogonalization procedure where only a small number of large eigenvalues, computed from the covariance matrix, are used to describe the variance in the random field (Liu, Belytschko and Mani 1987). The

dimension of $\boldsymbol{b}$ is reduced by the number of eigenvalues discarded, thus reducing the number of time integrations.

Further, note that the effective stiffness matrix in Equations 15–17 remains unchanged; therefore, only one factorization of the stiffness matrix is required. Furthermore, response kinematics and their differentials with respect to the elements of $\boldsymbol{b}$ are used in the "force vector" of each subsequent equation, and thus Equations 15–17 could most efficiently be solved in parallel. If analytical differentiation is possible, then the entire probabilistic finite element method requires $q+2$ time integrations: one to solve the zeroeth–order equation; q to solve for the sensitivity vectors and one more to solve the second–order equation. For certain non–linear systems analytical differentiation with respect to the elements of $\boldsymbol{b}$ is impossible and explicit numerical differentiation techniques, such as the central difference method, are required (Liu, Belytschko & Mani 1985). Similar procedures can also be developed to compute the probabilistic distributions of stresses, but this method can prove computationally expensive (Liu, Belytschko and Mani 1985).

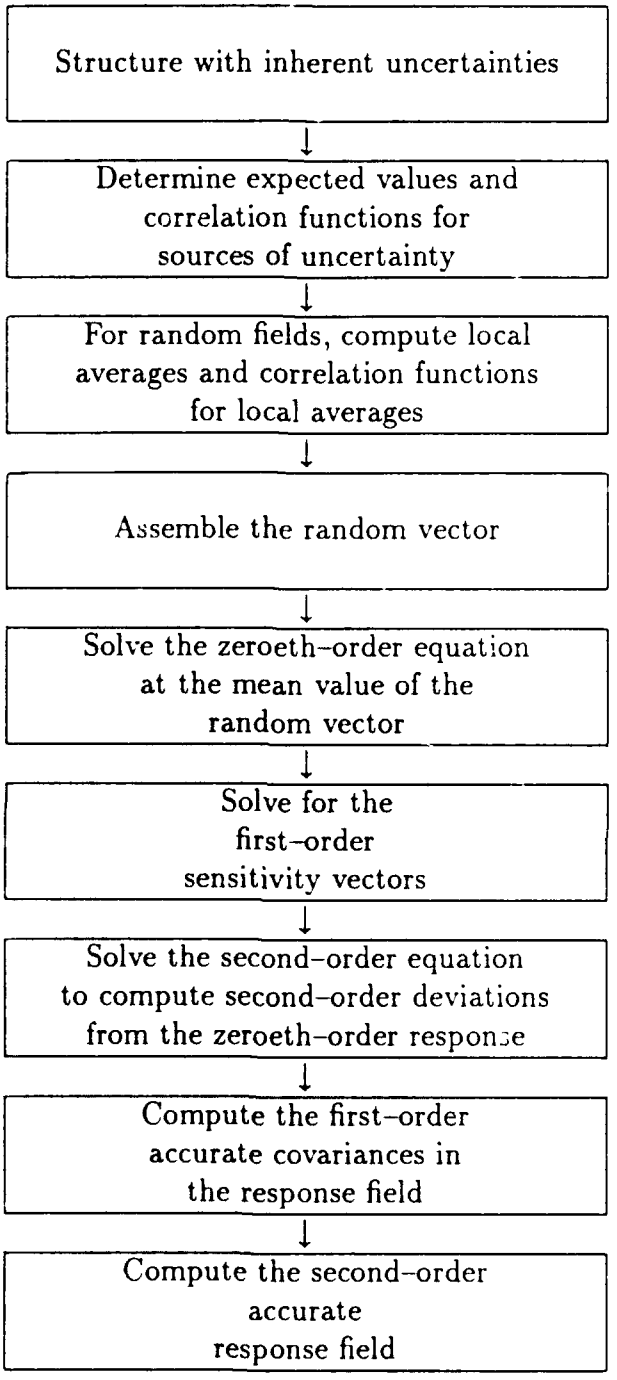

Figure 3: Schematic of the probabilistic finite element method.

3 SIMPLE ILLUSTRATIVE EXAMPLE

A random two-degree of freedom system is used to demonstrate the second-moment analysis method. The Monte Carlo simulation technique is used to provide a means of assessing the accuracy of the second-moment predictions. The problem statement as presented by Liu, Belytschko and Mani (1985) is shown in Figure 4, where the stiffness of each spring is described by a normal random variable. A second-moment analysis is performed to estimate the first and second-order expected values and variance in the response vector, and a Monte Carlo simulation is employed to assess these results.

The harmonic excitation, $F(t)$, and masses, m_1 and m_2, are deterministic parameters, whereas, the spring constants, k_1 and k_2, are described by independent normal distributions. The coefficient of variation for both spring constants is 0.05. The stiffness matrix can be expressed as

$$\boldsymbol{K} = \begin{bmatrix} k_1 + k_2 & -k_2 \\ -k_2 & k_2 \end{bmatrix}. \tag{25}$$

There is some question as to how the damping matrix was computed in the original paper. For this study 3% proportional damping is assumed such that the damping matrix is equal to

$$\boldsymbol{C} = \alpha \begin{bmatrix} m_1 & \\ & m_2 \end{bmatrix} + \beta \begin{bmatrix} k_1 + k_2 & -k_2 \\ -k_2 & k_2 \end{bmatrix}, \tag{26}$$

where the coefficients, α and β, are evaluated by uncoupling the equations of motion and computing α and β such that the equations $2\xi\omega_{n_i} = \alpha + \beta\omega_{n_i}^2$ are satisfied, where $i = 1, 2$, ξ is the proportion to critical damping and is equal to 3% and ω_{n_i} is the i^{th} natural frequency of the system. The natural frequencies are 5,124 rad/sec and 10,904 rad/sec. The coefficients, α and β, are computed as

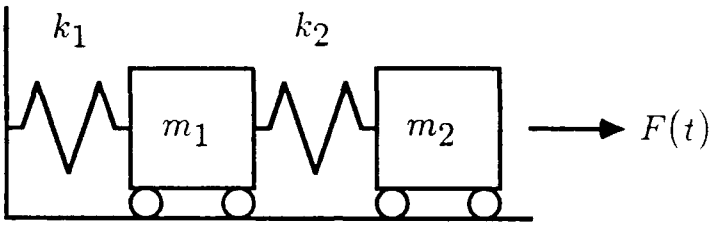

$m_1 = 0.372$ lb·sec^2/in

$m_2 = 0.248$ lb·sec^2/in

$F(t) = 25.0 \times 10^6 \sin(2000t)$ lb

$\mathrm{E}[k_1] = 24 \times 10^6$ lb/in

$\mathrm{E}[k_2] = 12 \times 10^6$ lb/in

$\sigma^2_{k_1} = 1.44 \times 10^{12}$ (lb/in)^2

$\sigma^2_{k_2} = 0.36 \times 10^{12}$ (lb/in)^2

Figure 4: Random 2–DOF oscillator.

209.15 and 3.7434×10^{-6}, respectively.

The random vector denoted by $\boldsymbol{k}$ represents the distributions of the spring stiffnesses. Note that the covariance between k_i and k_j is equal to zero. The equation of motion for this probabilistic system is

$$\boldsymbol{M}\ddot{\boldsymbol{x}}(\boldsymbol{k},t) + \boldsymbol{C}(\boldsymbol{k})\dot{\boldsymbol{x}}(\boldsymbol{k},t) + \boldsymbol{K}(\boldsymbol{k})\boldsymbol{x}(\boldsymbol{k},t) = \boldsymbol{F}(t). \tag{27}$$

The zeroeth-order equation is evaluated at $\bar{\boldsymbol{k}}$ and computed as follows

$$\boldsymbol{M}\ddot{\bar{\boldsymbol{x}}}(t) + \bar{\boldsymbol{C}}\dot{\bar{\boldsymbol{x}}}(t) + \bar{\boldsymbol{K}}\bar{\boldsymbol{x}}(t) = \boldsymbol{F}(t). \tag{28}$$

A second-moment analysis is performed to evaluate the following: 1) zeroeth-order mean response vectors; 2) sensitivity vectors; 3) variance in response vectors and 4) second-order mean response vectors. Equation 28 is evaluated to obtain the zeroeth-order kinematics. Sensitivity vectors are obtained by differentiating both sides of Equation 27 with respect to k_i, evaluating the differentials of the system matrices at $\bar{\boldsymbol{k}}$, and solving the resulting differential equations. Differentiating with respect to k_i and rearranging terms such that the sensitivity vectors are on the left-hand side of the equation, the sensitivity vectors are computed from the following first-order formula

$$\boldsymbol{M}\left.\frac{\partial\ddot{\boldsymbol{x}}(t)}{\partial k_i}\right|_{\bar{\boldsymbol{k}}} + \bar{\boldsymbol{C}}\left.\frac{\partial\dot{\boldsymbol{x}}(t)}{\partial k_i}\right|_{\bar{\boldsymbol{k}}} + \bar{\boldsymbol{K}}\left.\frac{\partial\boldsymbol{x}(t)}{\partial k_i}\right|_{\bar{\boldsymbol{k}}} = -\left\{\left.\frac{\partial\boldsymbol{C}}{\partial k_i}\right|_{\bar{\boldsymbol{k}}}\dot{\bar{\boldsymbol{x}}}(t) + \left.\frac{\partial\boldsymbol{K}}{\partial k_i}\right|_{\bar{\boldsymbol{k}}}\bar{\boldsymbol{x}}(t)\right\}, \tag{29}$$

where

$$\frac{\partial\boldsymbol{K}}{\partial k_1} = \begin{bmatrix} 1 & 0 \\ 0 & 0 \end{bmatrix}, \tag{30}$$

$$\frac{\partial\boldsymbol{K}}{\partial k_2} = \begin{bmatrix} 1 & -1 \\ -1 & 1 \end{bmatrix}, \tag{31}$$

$$\frac{\partial C}{\partial k_1} = \beta \begin{bmatrix} 1 & 0 \\ 0 & 0 \end{bmatrix}, \tag{32}$$

and

$$\frac{\partial C}{\partial k_2} = \beta \begin{bmatrix} 1 & -1 \\ -1 & 1 \end{bmatrix}. \tag{33}$$

Zeroeth–order estimates of mean response kinematics are determined using the Newmark time integration method (Bathe 1982). The variance in the zeroeth–order response of $x_l(t)$ is computed from the first–order equation

$$\mathrm{var}[x_l(t)] \approx \sum_{i=1}^{2} \left\{ \left(\left. \frac{\partial x_l(t)}{\partial k_i} \right|_{\bar{\boldsymbol{k}}} \right)^2 \mathrm{var}[k_i] \right\}. \tag{34}$$

The second–order mean response vectors are computed by solving the second–order equation

$$\boldsymbol{M}\Delta\ddot{\bar{\boldsymbol{x}}}(t) + \bar{\boldsymbol{C}}\Delta\dot{\bar{\boldsymbol{x}}}(t) + \bar{\boldsymbol{K}}\Delta\bar{\boldsymbol{x}}(t) =$$

$$-\sum_{i=1}^{2} \left\{ \left(\left. \frac{\partial \boldsymbol{C}}{\partial k_i} \right|_{\bar{\boldsymbol{k}}} \left. \frac{\partial \dot{\boldsymbol{x}}(t)}{\partial k_i} \right|_{\bar{\boldsymbol{k}}} + \left. \frac{\partial \boldsymbol{K}}{\partial k_i} \right|_{\bar{\boldsymbol{k}}} \left. \frac{\partial \boldsymbol{x}(t)}{\partial k_i} \right|_{\bar{\boldsymbol{k}}} \right) \mathrm{var}[k_i] \right\}, \tag{35}$$

and the expected value of the response vector, accurate to second–order, is

$$\mathrm{E}[\boldsymbol{x}(\boldsymbol{k},t)] \approx \bar{\boldsymbol{x}}(t) + \Delta\bar{\boldsymbol{x}}(t). \tag{36}$$

A Monte Carlo simulation is also performed to estimate the expected value and variance in the response vectors. Two independent normal distributions of random spring stiffnesses are generated, each with 400 samples, and each pair of random stiffnesses is substituted into the equation of motion to compute a distribution of response vectors. After 400 time integrations have been completed the mean, mean squared and variance in the response of $x_l(t)$ can be computed

as

$$\mathrm{E}[x_l(t)] = \frac{1}{400}\sum_{i=1}^{400} x_{l_i}(t) \tag{37}$$

$$\mathrm{E}[(x_l(t))^2] = \frac{1}{400}\sum_{i=1}^{400} (x_{l_i}(t))^2 \tag{38}$$

$$\mathrm{var}[x_l(t)] = \mathrm{E}[(x_l(t))^2] - \mathrm{E}[x_l(t)]^2. \tag{39}$$

The results from the second–moment analysis and Monte Carlo simulations are plotted in Figures 5–8. Figures 5 and 6 indicate the zeroeth–order and second–order response of $x_1(t)$ and $x_2(t)$, respectively, and the expected response predicted by the Monte Carlo simulation. The differences between the second–order mean response and the mean response predicted using the Monte Carlo method are negligible, but there is a notable difference between these two estimates of mean response and the zeroeth–order response. The standard deviation in response estimates of $x_1(t)$ and $x_2(t)$ is shown in Figures 7 and 8, respectively The second–moment analysis estimates tend to overshoot those obtained using Monte Carlo simulations at large times. This phenomena is a result of resonant excitation in the first–order equation, Equation 29, which estimates the sensitivity vectors (Liu, Belytschko and Mani 1985). The resonant excitation is present in Equation 29 because the natural frequencies of Equations 28 and 29 are identical and the kinematics obtained by solving Equation 28 are used in the excitation of Equation 29. The kinematics predicted by Equation 28 thus reflect the natural frequency of the system and act as a resonant excitation.

The resonant excitation is present in all equations above the zeroeth–order. However, it is negligible in structures with a large amount of damping and in analyses which do not extend to large times where steady state response is prevalent (Liu, Belytschko and Mani 1985). A technique based on Fourier analysis has been

developed to remove these secular terms from higher–order response estimates (Liu, Besterfield and Belytschko 1986).

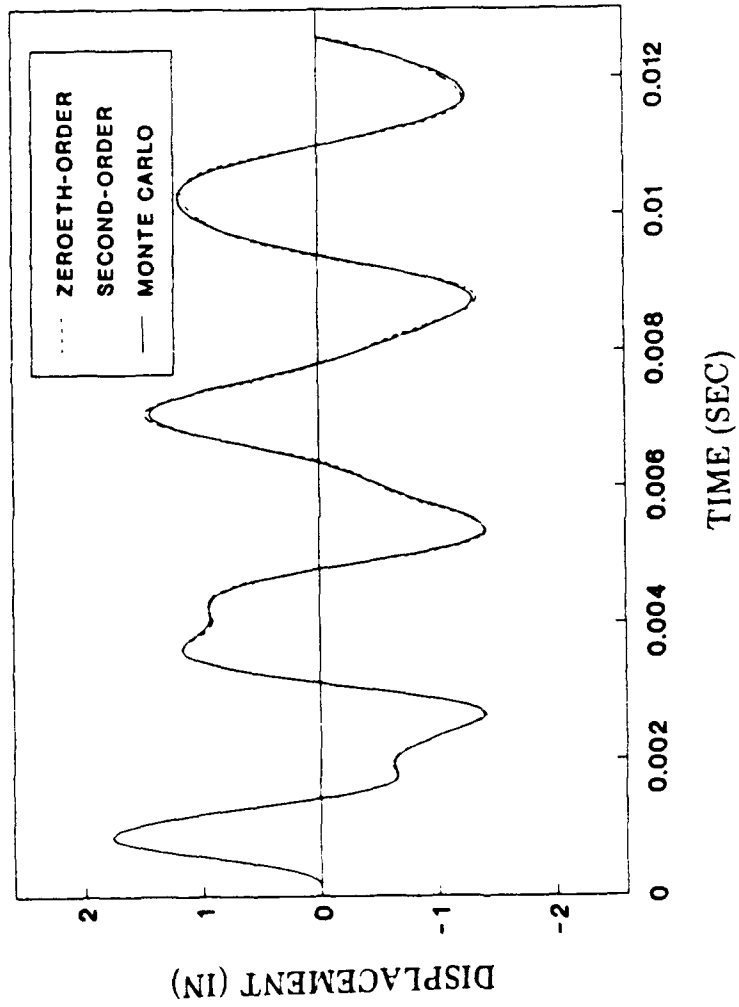

Figure 5: Displacement of node 1 of 2-DOF oscillator.

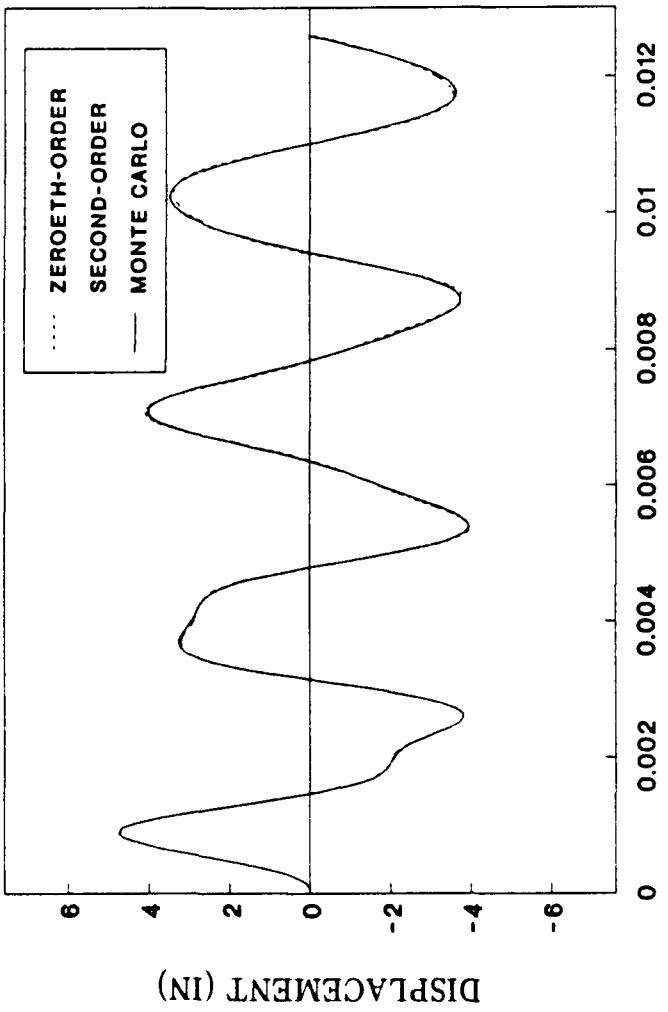

Figure 6: Displacement of node 2 of 2-DOF oscillator.

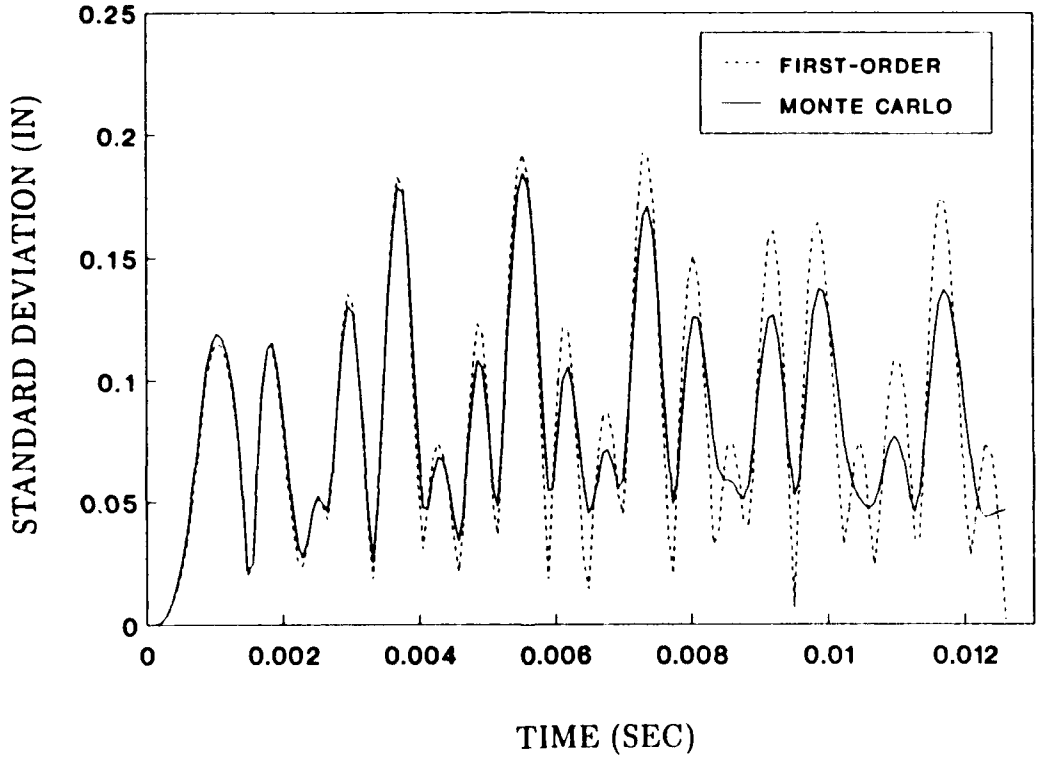

Figure 7: Standard deviation in displacement of node 1 of 2-DOF oscillator.

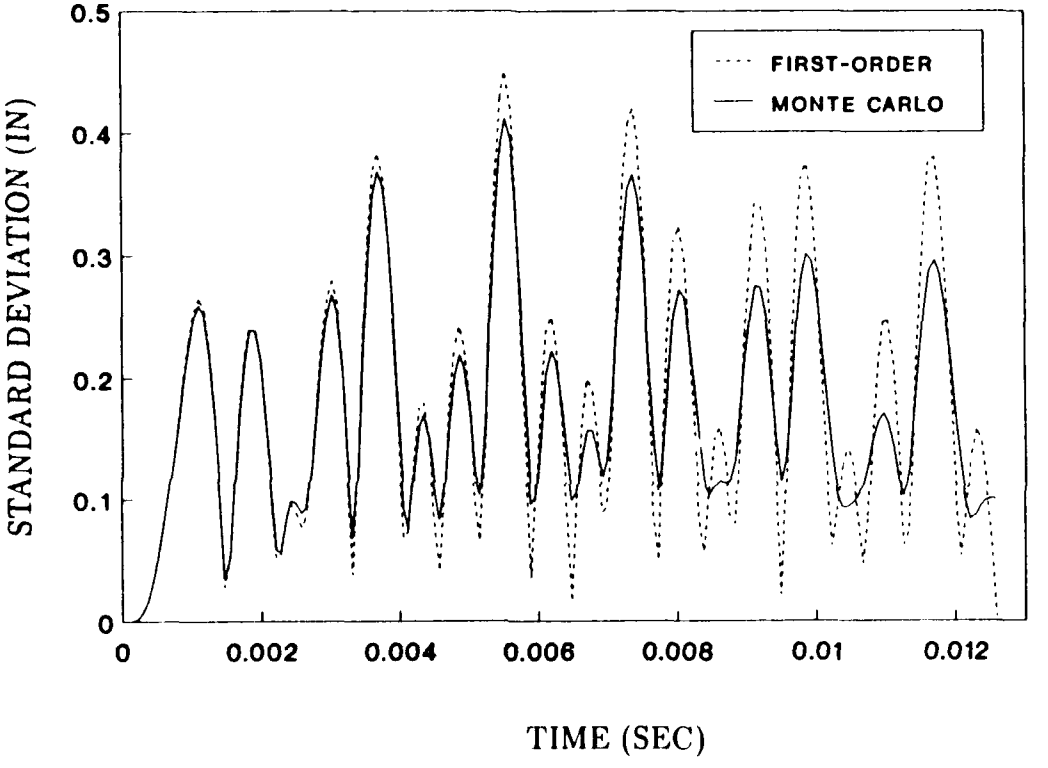

Figure 8: Standard deviation in displacement of node 2 of 2-DOF oscillator.

4 APPLICATION OF PROBABILISTIC FINITE ELEMENT METHODS TO MARINE RISER ANALYSES

Marine drilling risers are an integral part of offshore drilling operations. They are used to enclose and protect the drill string and provide a path by which the drilling mud can reach the surface. A typical riser consists of interconnected sections of steel pipe, kept in tension, which extend from the riser support ring on the drill ship to the lower ball joint slightly above the sea floor. A drilling riser is depicted in Figure 9 where the riser is modeled as a beam which is pin-connected at both the lower ball joint and riser support ring and constrained to respond with the vessel motions at the riser support ring. Choke and kill lines are externally connected to the riser, and buoyant material is generally added for deep water risers. Response and stress envelopes are generated for engineering design of marine drilling risers, where the envelope represents the maximum and minimum values of the riser displacements and stresses. These values are then compared with the allowable displacements and stresses obtained from established design codes.

Marine drilling risers are commonly analyzed using finite element techniques (Chakrabarti and Frampton 1982). These analyses are deterministic and typically neglect the randomness associated with the material properties and the external loading. Specifically, uncertainties in riser analyses can include stochastic excitation, tension in the riser, and structural and mud properties. Linear stochastic techniques which incorporate random wind, wave and foundation excitation have been well developed for the finite element method and are commonly employed in riser analyses. Both linear and nonlinear frequency domain analyses have been employed to predict the statistical moments in riser displacements and stresses.

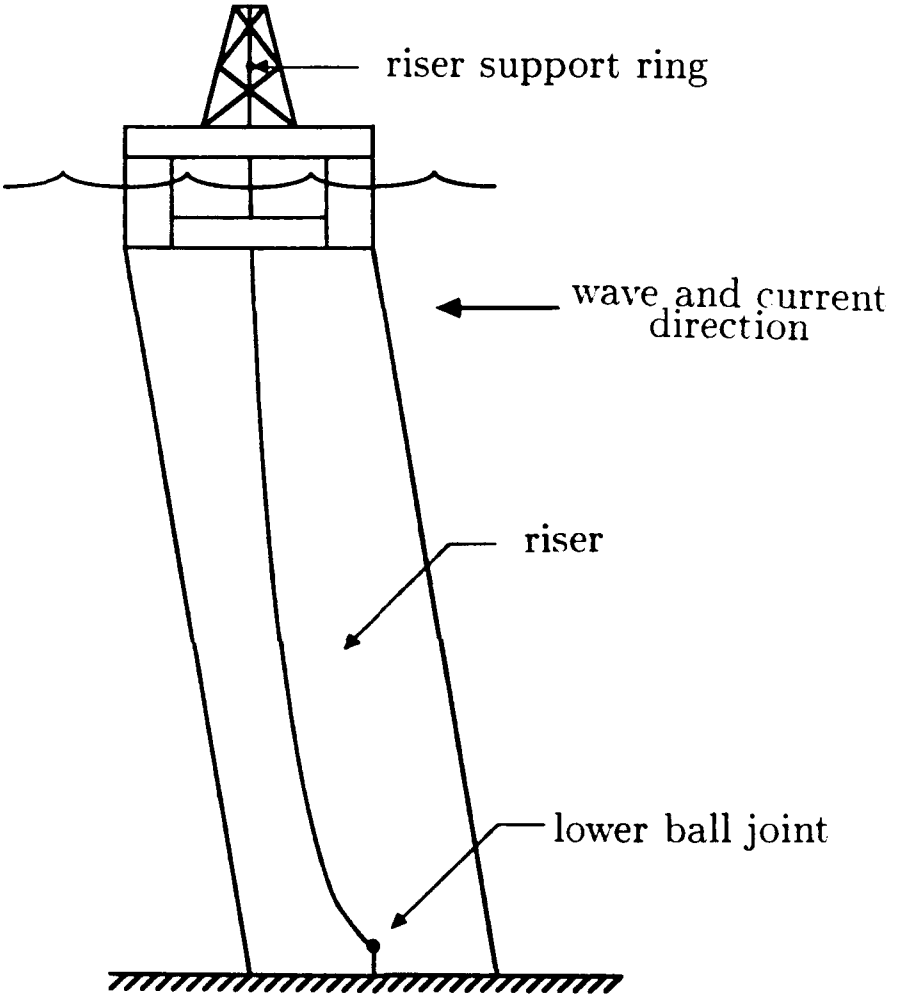

Figure 9: Marine drilling riser

In linear analyses only the first–order approximation of the hydrodynamic drag force spectra is considered and relative motion between the structure and the wave is neglected. The numerical simulations involved in nonlinear frequency domain analyses of marine risers are significantly more complicated than those for linear analyses. Nonlinear stochastic analyses can include higher–order approximations of the drag force spectra (Niedzwecki and Leder 1990) and relative motion (Sandt and Niedzwecki 1990). Time domain analyses do not require linearization of the equation of motion and can be used to assess the probabilistic distributions of displacements and stresses and to estimate extreme return period events. Comparative studies have been performed which demonstrate the range in response and stress predictions of analogous riser simulations using various industrial finite element procedures (API 1977).

Sources of uncertainty related to structural properties have received far less attention than those related to the stochastic excitation and, in general, are either assumed small and ignored, or conservative estimates are employed throughout analyses. As drilling progresses into extreme water depths these latter sources of randomness could necessitate a probabilistic analysis of the riser, particularly if composites which are known to possess highly random material properties become a viable alternative to steel.

In this chapter the second–moment analysis, as developed in Chapter 2, in combination with finite element techniques, is specifically developed for a probabilistic analysis of an offshore drilling riser. Monte Carlo simulations are also employed as a means of comparing results. An assessment of the significance of inclusion of sources of uncertainty on the distributions of response behavior, excluding stochastic excitation, is also made.

4.1 Finite Element Model

4.1.1 Formulation of the Equation of Motion

The governing equations adapted for this study are based on those for a vibrating uniform beam with linear variations in axial tension (Gardner & Kotch 1976). The approach incorporates axial tension and compression effects and ignores shear effects. Assumptions regarding the finite element solution require:

i) the angle between the riser and vertical axis remain below ten degrees;

ii) choke and kill lines externally attached to the riser do not contribute to the bending stiffness and

iii) effects of the drill string, kept in constant tension, are ignored and variations in top tension propagate instantaneously throughout the riser.

The finite element equations which directly follow are developed within a deterministic framework and then the probabilistic formulations are incorporated.

A differential riser element of length Δz is shown in Figure 10, where for simplicity, the choke and kill lines are not shown and the element is considered completely immersed in water and filled with mud. The water depth is denoted as d and the mud column is assumed to span the entire length of the riser, L. The specific weights of the water, mud, and riser pipe are defined as γ_w, γ_m and γ_p, respectively. The riser is attached to the lower ball joint at an elevation, z_0, above the sea floor and the displacement at any point on the riser at elevation z above the sea floor at time t is denoted as $x(z,t)$. Externally, the riser is subject to hydrostatic pressure, a static current force, $f_c(z)$, and hydrodynamic wave loads, $f_w(z,t)$. The internal walls of the riser are also subject to static pressure resulting from the mud column. The riser is initially pre-tensioned at the riser support ring to some value T_{top} in order to support the net weight and to increase the stiffness.

The tension in a section of riser consists of two components: a constant tensile force, T_0, and a linearly varying tensile force due to an increase in tension with elevation required to support the net weight. The linearly varying tensile force can be visualized by considering Figure 10, where at the bottom of the differential element the linearly varying tensile force is zero and at the top of the differential element it has a value of $(\gamma_p A_p + \gamma_m A_i)\Delta z$. The variables A_p and A_i represent the cross-sectional area of the riser material and the internal area of the riser, respectively.

Integration of the pressures over the surfaces upon which they act, addition of inertial loads, imposition of equilibrium equations and employment of Bernoulli-Euler beam theory yields

$$\frac{1}{g}[\gamma_p A_p + \gamma_m A_i - (C_M - 1)\gamma_w A_e]\ddot{x}(z,t) + EI\frac{\partial^4 x(z,t)}{\partial z^4}$$

$$- \{T_{top} - (\gamma_p A_p + \gamma_m A_i)[L - (z - z_0)] + \gamma_w A_o(d - z)\}\frac{\partial^2 x(z,t)}{\partial z^2}$$

$$- [(\gamma_p A_p + \gamma_m A_i) - \gamma_w A_o]\frac{\partial x(z,t)}{\partial z} = f_c(z) + f_w(z,t), \qquad (40)$$

where g is the gravitational coefficient, A_e is the effective hydrodynamic diameter, E is the modulus of the pipe, I is the moment of inertia of the pipe and C_M is the added mass coefficient. Equation 40 can be simplified to the governing equation of a vibrating uniform beam with a linearly varying axial tension

$$\bar{m}\ddot{x}(z,t) + EI\frac{\partial^4 x(z,t)}{\partial z^4} - \frac{\partial}{\partial z}\left[(T_0 + T'z)\frac{\partial x(z,t)}{\partial z}\right] = f_c(z) + f_w(z,t), \qquad (41)$$

where $\bar{m}$ represents the effective mass per length of the riser and T' represents the derivative of the linearly varying tensile force with respect to z.

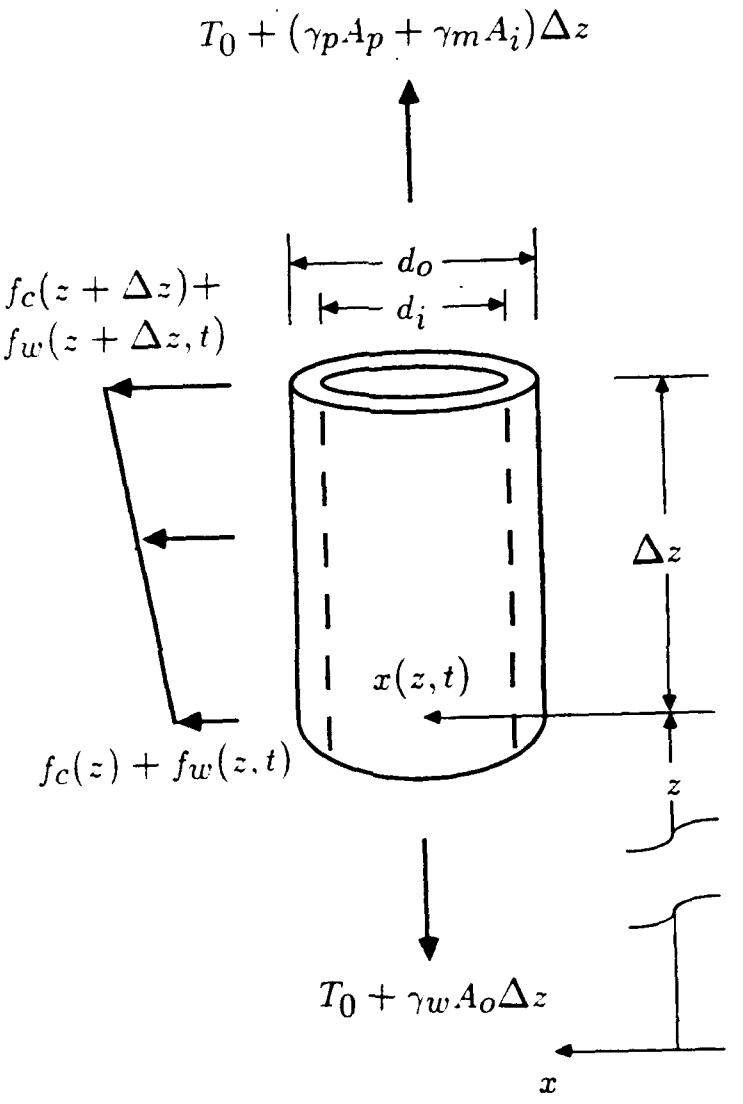

Figure 10: Differential element of marine drilling riser.

4.1.2 Finite Element Discretization

The Lagrange equations are employed to develop the discrete coupled forms of the equations motion. The work done by the external forces on a riser element of length ℓ is equal to the total of the potential and kinetic energy. Thus

$$\int_0^\ell \{[f_c(z) + f_w(z,t)]x(z,t)\}\, dz =$$

$$\frac{1}{2}\int_0^\ell \left\{ EI[\frac{\partial^2 x(z,t)}{\partial z^2}]^2 + (T_0 + T'z)[\frac{\partial x(z,t)}{\partial z}]^2 \right\} dz +$$

$$\frac{1}{2}\int_0^\ell \left\{ \bar{m}[\dot{x}(z,t)]^2 \right\} dz. \tag{42}$$

A discrete element coordinate system, where x_i represents the displacement at degree of freedom i, is chosen as depicted in Figure 11 such that the deformation of the riser element at z is approximated as

$$x(z,t) = \sum_{i=1}^{4} \phi_i(z) x_i(t), \tag{43}$$

where the element shape functions, $\phi_i(z)$, are defined as follows

$$\phi_1(z) = 1 - 3\left(\frac{z}{\ell}\right)^2 + 2\left(\frac{z}{\ell}\right)^3 \tag{44}$$

$$\phi_2(z) = z\left[1 - \left(\frac{z}{\ell}\right)\right]^2 \tag{45}$$

$$\phi_3(z) = 3\left(\frac{z}{\ell}\right)^2 - 2\left(\frac{z}{\ell}\right)^3 \tag{46}$$

$$\phi_4(z) = z\left[\left(\frac{z}{\ell}\right)^2 - \left(\frac{z}{\ell}\right)\right]. \tag{47}$$

Substituting Equation 43 into Equation 42 and employing the Lagrange equations yields the discrete coupled element equations of motion.

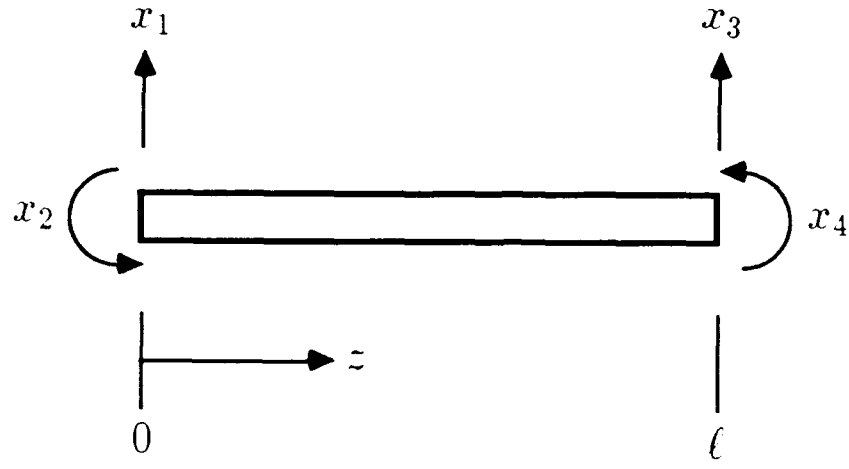

Figure 11: Element coordinate system and nodal degrees of freedom.

4.1.3 Development of the Mass and Stiffness Matrices

The elements in the mass matrix are computed by evaluating the integral

$$m_{ij} = \int_0^\ell \bar{m}\phi_i(z)\phi_j(z)\,dz. \tag{48}$$

The resulting symmetrical element mass matrix can be expressed as

$$[m] = \frac{\bar{m}\ell}{420}\begin{bmatrix} 156 & 22\ell & 54 & -13\ell \\ & 4\ell^2 & 13\ell & -3\ell^2 \\ & & 156 & -22\ell \\ & & & 4\ell^2 \end{bmatrix}, \tag{49}$$

where $\bar{m}$ is the effective mass per length. It is dependent upon whether or not the element is submerged and is computed as

$$\bar{m} = \begin{cases} \bar{m}_p + \bar{m}_m + \bar{m}_a & \text{for } z < d \\ \bar{m}_p + \bar{m}_m & \text{for } z \geq d \end{cases}, \tag{50}$$

where the mass per unit length of the riser and mud and the added mass are denoted $\bar{m}_p$, $\bar{m}_m$ and $\bar{m}_a$, respectively.

The element stiffness matrix is divided into three components which include contributions from the bending stiffness, the average constant tension and the linear variation in tension. This can be expressed as

$$k_{ij} = EI\int_0^\ell \phi_i''(z)\phi_j''(z)\,dz$$

$$+ T_0\int_0^\ell \phi_i'(z)\phi_j(z)dz + T'\int_0^\ell \phi_i'(z)\phi_j(z)z\,dz. \tag{51}$$

The element stiffness matrix can be evaluated by integrating each of the components to obtain the appropriate matrix expressions. Adding these together yields the final element stiffness matrix. The element bending stiffness matrix is found to be

$$[k]_{EI} = \frac{2EI}{\ell^3}\begin{bmatrix} 6 & 3\ell & -6 & 3\ell \\ & 2\ell^2 & -3\ell & \ell^2 \\ & & 6 & -3\ell \\ & & & 2\ell^2 \end{bmatrix}. \tag{52}$$

The constant tension element stiffness matrix is computed at the bottom node of the element relative to the sea floor. Evaluating the second term in Equation 51 yields the following expression

$$[k]_{T_0} = \frac{T_0}{30\ell}\begin{bmatrix} 36 & 3\ell & -36 & 3\ell \\ & 4\ell^2 & -3\ell & -\ell^2 \\ & & 36 & -3\ell \\ & & & 4\ell^2 \end{bmatrix}, \tag{53}$$

where

$$T_0 = \begin{cases} T_{top} - \{(\gamma_p A_p + \gamma_m A_i)[L - (z - z_0)]\} \\ +\gamma_w A_o(d - z) & \text{for } z < d \\ \\ T_{top} - \{(\gamma_p A_p + \gamma_m A_i)[L - (z - z_0)]\} & \text{for } z \geq d \end{cases}. \tag{54}$$

Finally, the element stiffness matrix accounting for contributions from the linear variation in axial tension is computed by evaluating the third term in Equation 51 as follows

$$[k]_{T'} = T'\begin{bmatrix} \frac{3}{5} & \frac{\ell}{10} & -\frac{3}{5} & 0 \\ & \frac{\ell^2}{30} & -\frac{\ell}{10} & -\frac{\ell^2}{60} \\ & & \frac{3}{5} & 0 \\ & & & \frac{\ell^2}{10} \end{bmatrix}, \tag{55}$$

where

$$T' = \begin{cases} \gamma_p A_p + \gamma_m A_i - \gamma_w A_o & \text{for } z < d \\ \gamma_p A_p + \gamma_m A_i & \text{for } z \geq d \end{cases}. \tag{56}$$

The total element stiffness matrix can now be assembled, that is

$$[k] = [k]_{EI} + [k]_{T_0} + [k]_{T'}. \tag{57}$$

After evaluating the mass and stiffness matrices for all of the elements, the global mass and stiffness matrices are assembled. The global mass matrix is denoted as

$\boldsymbol{M}$ and the global stiffness matrix is denoted as $\boldsymbol{K}$.

4.1.4 Development of the Damping Matrix

Structural damping is incorporated into the solution of the marine riser system by introducing Rayleigh proportional damping (James, Smith, Wolford and Whaley 1989). The damping matrix, $\boldsymbol{C}$, is assumed to be of the form $\alpha\boldsymbol{M}+\beta\boldsymbol{K}$. For simplicity with regard to the probabilistic formulations which follow, the coefficients, α and β, are evaluated by predicting, in a least squared sense, the best fit to the equation $2\xi_i\omega_{n_i} = \alpha + \beta\omega_{n_i}^2$ where the variables ξ_i and ω_{n_i} respectively, represent the proportion to critical damping and the natural frequency of the ith mode. For the cases examined in this thesis, ξ_i is assumed to be constant for the first four modes, and only the first four natural frequencies are used to approximate the coefficients, α and β. The predicted modal damping values for the first four modes, computed using the estimates of α and β, are approximately equal to the actual values. For higher modes the predicted modal damping values are less than the actual values.

4.1.5 Development of the Force Vector

If the external forces are assumed to vary linearly over the elements, then the external force vector, $\tilde{F}_i(t)$, for element degree of freedom i is approximated by evaluating the following integral

$$F_i(t) = f_0(t)\int_0^\ell \phi_i(z)dz + f'(t)\int_0^\ell \phi_i(z)z\,dz, \tag{58}$$

where $f_0(t)$ is the constant force per unit length over the element and $f'(t)$ is the linear variation in the force per unit length. The element force vector is thus computed as

$$\tilde{F}(t) = \left\{ \begin{array}{c} \frac{\ell}{2} f_0(t) + 0.15\ell^2 f'(t) \\ \frac{\ell^2}{12} f_0(t) + \frac{\ell^3}{30} f'(t) \\ \frac{\ell}{2} f_0(t) + 0.35\ell^2 f'(t) \\ -\frac{\ell^2}{2} f_0(t) - \frac{\ell^3}{20} f'(t) \end{array} \right\}. \tag{59}$$

For the analyses performed in this study, element lengths are small enough such that all components of the external force, the current, inertial and drag forces can be considered to vary linearly over each element. The current force per unit length which results from a steady current is

$$f_c(z) = k_D u_c(z), \tag{60}$$

where $u_c(z)$ is the velocity of the current and the constant, k_D, is equal to $\frac{1}{2g}\gamma_w C_D d_e$, where C_D is the drag coefficient and d_e is the effective hydrodynamic diameter. The inertial force per unit length is

$$f_I(z,t) = \frac{1}{4g} C_M \gamma_w \pi d_e^2 \dot{u}(z,t), \tag{61}$$

where C_M is the inetrial force coefficient, and the drag force per unit length is

$$f_D(z,t) = k_D[u(z,t) - \dot{x}(z,t)]\,|u(z,t) - \dot{x}(z,t)|\,, \tag{62}$$

where $u(z,t)$ and $\dot{u}(z,t)$ are the horizontal velocity and acceleration components of the wave. Note that the velocity of the structure appears in the nonlinear hydrodynamic drag force term. This is a result of the relative motion between the structure and wave and introduces hydrodynamic damping into the system.

Once the element force vectors have been computed by substitution of each of the force expressions into Equation 59, the global force vectors can be assembled.

The global steady current vector is $\boldsymbol{F}_c$. The time dependant global wave force vector is $\boldsymbol{F}_w(t)$ and includes the inertial force vector, $\boldsymbol{F}_I(t)$, and the drag force vector, $\boldsymbol{F}_D(t)$.

The top node of the riser corresponding to the riser support ring is considered to respond with the surge motion of the drill ship. The penalty method is used to impose these translations (Bathe 1982, McCoy 1985). A fictitious stiffness several orders of magnitude larger than the element in the global stiffness matrix corresponding to the degree of freedom of the imposed top translation is added to the element in the global stiffness matrix corresponding to the degree of freedom of the imposed top translation. Thus, for a specified displacement at the global degree of freedom $\imath$, the corresponding element in the stiffness matrix can be computed as

$$K_{\imath\imath} = K_{\imath\imath} + \kappa K_{\imath\imath}, \tag{63}$$

where κ is a large constant. The product of the fictitious stiffness and the specified displacement are also added to the element of the force vector corresponding to the degree of freedom of the imposed top translation. The element in the force vector corresponding to the degree of freedom of the specified displacement can be computed as

$$F_\imath(t) = F_\imath(t) + \kappa K_{\imath\imath}\epsilon(t), \tag{64}$$

where $\epsilon(t)$ represents the specified displacement. A new global force vector is defined which represents the horizontal force necessary to produce the specified displacement. The new vector, $\boldsymbol{F}_\epsilon(t)$, is expressed as

$$\boldsymbol{F}_\epsilon(t) = \left\{ \begin{array}{ccccccc} 0 & 0 & \ldots & \kappa K_{\imath\imath}\epsilon(t) & \ldots & 0 & 0 \end{array} \right\}^{\mathrm{T}}, \tag{65}$$

where all terms are zero except for the force expression at the degree of freedom corresponding to the specified displacement.

4.1.6 Solution to the Finite Element Equations

The discretized finite element equation of motion can now be written as

$$\boldsymbol{M}\ddot{\boldsymbol{x}}(t) + \boldsymbol{C}\dot{\boldsymbol{x}}(t) + \boldsymbol{K}\boldsymbol{x}(t) = \boldsymbol{F}_c + \boldsymbol{F}_w(t) + \boldsymbol{F}_e(t). \tag{66}$$

For numerical simulations the static and dynamic components in Equation 66 are segregated. The static equation is written as

$$\boldsymbol{K}\boldsymbol{x}_s = \boldsymbol{F}_c + \boldsymbol{F}_e(0), \tag{67}$$

where $\boldsymbol{x}_s$ is the vector representing the static offset. The equation of motion which contains only the dynamic components of Equation 66 can be expressed as

$$\boldsymbol{M}\ddot{\boldsymbol{x}}_d(t) + \boldsymbol{C}\dot{\boldsymbol{x}}_d(t) + \boldsymbol{K}\boldsymbol{x}_d(t) = \boldsymbol{F}_w(t) + \boldsymbol{F}_e(t) - \boldsymbol{F}_e(0), \tag{68}$$

where $\boldsymbol{x}_d(t)$ represents the displacement vector resulting from the hydrodynamic wave force contributions. The total dynamic response of the riser, $\boldsymbol{x}(t)$, is thus $\boldsymbol{x}_s + \boldsymbol{x}_d(t)$.

The Newmark method is employed to solve Equation 68 for the structural kinematics (Newmark 1959, Bathe 1982). As a result of relative motion, the nonlinear drag force contributions to the wave force vector are functions of the velocity of the structure. An iterative approach to the solutions for the kinematic vectors is required if the governing equations are not linearized. The Newmark method can be modified to iterate until the velocity vectors converge. The algorithm of the steps required to compute the structural kinematics at time t_i is shown below.

1.) Compute the kinematic vectors at time t_i, where the dynamic force vector is assembled assuming that the velocity of the structure can be computed from $\dot{\boldsymbol{x}}_d(t_{i-1})$.

2.) If the new estimate of the velocity vector converges with the old estimate, then increment the time step.

3.) If the new estimate of the velocity vector does not converge with the old estimate, then reassemble the force vector using the new velocity estimates and recompute the kinematic vectors.

4.) Repeat steps 2 and 3 as necessary.

4.2 Applications of Response Predictions

4.2.1 Stress Estimates

The response vector, $\boldsymbol{x}(t)$, computed using the finite element method can be used to predict the stresses in the riser at time t. The maximum bending stress in the outer wall of the riser can be computed from the general equation $\sigma = \frac{Mc}{I}$, where σ is the bending stress, c is the radius to the outer wall of the riser and M is the bending moment. The bending moment, $M(z,t)$, can be computed at elevation z and time t using the following equation

$$M(z,t) = \frac{EI}{\rho(z,t)}, \tag{69}$$

where $\rho(z,t)$ is the radius of curvature. The radius of curvature can be obtained from the following expression

$$\frac{1}{\rho(z,t)} = \frac{\partial^2 x(z,t)}{\partial z^2} = \frac{\partial \theta(z,t)}{\partial z}, \tag{70}$$

where $\theta(z,t)$ is the rotation of the riser in the x–z plane. The expression $\frac{\partial \theta(z,t)}{\partial z}$ can be evaluated at the midpoint of element l using the numerical approximation

$$\left.\frac{\partial\theta(z,t)}{\partial z}\right|_{z_l} \approx \frac{\theta(z_l+\Delta z_l,t)-\theta(z_l-\Delta z_l,t)}{2\Delta z_l}, \tag{71}$$

where z_l is the vertical coordinate of the midpoint of element l and $2\Delta z_l$ is the length of element l. The expressions $\theta(z_l+\Delta z_l,t)$ and $\theta(z_l-\Delta z_l,t)$ are the rotations at the top and bottom of element l, respectively. These are computed directly in the finite element solution. The stress at the midpoint of element l and at time t can now be approximated as

$$\sigma_l(t) \approx Ec\,\frac{\theta(z_l+\Delta z_l,t)-\theta(z_l-\Delta z_l,t)}{2\Delta z_l}. \tag{72}$$

4.2.2 Displacement and Stress Envelopes

Displacement and stress envelopes are required for the engineering design of marine risers. For this study these parameters are estimated during the steady state response of the riser. The maximum and minimum peak displacements are computed for each translational degree of freedom and the maximum and minimum peak stresses are computed at their respective elevations.

4.3 Second–Moment Solution Procedures Specific to the Marine Riser Problem

Once the finite element equations have been formulated, and the sources of uncertainty in the marine riser system have been identified, the second–moment method can be applied. The random vector, $\boldsymbol{b}$, must be formulated as described in Chapter 2 and then the probabilistic analysis is used to predict the first- and second–moments and the covariances in the discrete displacement fields. From these results, the expected values of the discrete stresses and approximations for

the variances in the stresses can be made.

4.3.1 Zeroeth–Order Predictions

The zeroeth–order kinematics are estimated after the expected values of the elements in the random vector are substituted into the appropriate finite element expressions. An approximation of the expected stress at the midpoint of element l is obtained by taking the expected value of both sides of Equation 72. The expected value for the stress at midpoint of element l is

$$\mathrm{E}[\sigma_l(t)] \approx \frac{Ec}{2\Delta z_l} \left\{ \mathrm{E}[\theta(z_l + \Delta z_l, t)] - \mathrm{E}[\theta(z_l - \Delta z_l, t)] \right\}, \tag{73}$$

where it is assumed that E and c are deterministic. If these parameters were random then they would be replaced by their expected values in Equation 73.

4.3.2 Evaluation of the Sensitivity Vectors

The sensitivity vectors for the response kinematics are computed as described in Chapter 2. The first–order equations are assembled by differentiating the riser finite element equation with respect to each element of the random vector and evaluating the resulting equations at $\bar{\boldsymbol{b}}$, where $\bar{\boldsymbol{b}}$ represents a vector whose elements are the expected values of the elements in $\boldsymbol{b}$. Each first–order equation is solved in terms of $\frac{\partial \boldsymbol{x}(t)}{\partial b_i}\Big|_{\bar{\boldsymbol{b}}}$, $\frac{\partial \dot{\boldsymbol{x}}(t)}{\partial b_i}\Big|_{\bar{\boldsymbol{b}}}$ and $\frac{\partial \ddot{\boldsymbol{x}}(t)}{\partial b_i}\Big|_{\bar{\boldsymbol{b}}}$, which represent the sensitivity in the response, velocity and acceleration vectors, respectively, to element b_i in the random vector.

Differentiation of the mass, damping and stiffness matrices with respect to each element in the random vector is required, and the differentials are evaluated at $\bar{\boldsymbol{b}}$. The procedure used in this study to evaluate the differentials was to differentiate

the element mass and stiffness matrices, evaluate the resulting expressions at $\bar{\boldsymbol{b}}$, and assemble the global matrices $\frac{\partial \boldsymbol{M}}{\partial b_i}\Big|_{\bar{\boldsymbol{b}}}$ and $\frac{\partial \boldsymbol{K}}{\partial b_i}\Big|_{\bar{\boldsymbol{b}}}$. The corresponding expression for the global damping matrix, $\frac{\partial \boldsymbol{C}}{\partial b_i}\Big|_{\bar{\boldsymbol{b}}}$, was then computed as $\alpha \frac{\partial \boldsymbol{M}}{\partial b_i}\Big|_{\bar{\boldsymbol{b}}} + \beta \frac{\partial \boldsymbol{K}}{\partial b_i}\Big|_{\bar{\boldsymbol{b}}}$.

Differentiation of the steady current force vector, the hydrodynamic inertia wave force vector, and the force vector used to produce the specified displacements is straightforward. The element force vectors are differentiated with respect to the elements in the random vector and evaluated at the expected values of the elements in the random vector. The global force vectors, $\frac{\partial \boldsymbol{F}_c}{\partial b_i}\Big|_{\bar{\boldsymbol{b}}}$, $\frac{\partial \boldsymbol{F}_{I(t)}}{\partial b_i}\Big|_{\bar{\boldsymbol{b}}}$ and $\frac{\partial \boldsymbol{F}_{\epsilon(t)}}{\partial b_i}\Big|_{\bar{\boldsymbol{b}}}$, are then assembled.

Differentiation of the nonlinear hydrodynamic drag force vector is more complicated. Recall that the general expression for the drag force per length, Equation 62, is

$$f_D(z,t) = k_D[u(z,t) - \dot{x}_d(z,t)]\,|u(z,t) - \dot{x}_d(z,t)|\,. \tag{74}$$

The drag force per length at the top and bottom of element l can be expressed in terms of their global coordinates, $f_{D_{2l+1}}(t)$ and $f_{D_{2l-1}}(t)$, respectively, where a representation of the displacements and drag force in the global coordinate system is shown in Figure 12. The horizontal velocities of the wave at the top and bottom of element l are $u_{2l+1}(t)$ and $u_{2l-1}(t)$, and the horizontal velocities of the structure at the top and bottom of element l are $\dot{x}_{2l+1}(t)$ and $\dot{x}_{2l-1}(t)$. The drag force per length at the top of element l can thus be written as

$$f_{D_{2l+1}}(t) = k_D[u_{2l+1}(t) - \dot{x}_{2l+1}(t)]\,|u_{2l+1}(t) - \dot{x}_{2l+1}(t)| \tag{75}$$

and the drag force per length at the bottom of element l can be written as

$$f_{D_{2l-1}}(t) = k_D[u_{2l-1}(t) - \dot{x}_{2l-1}(t)]\,|u_{2l-1}(t) - \dot{x}_{2l-1}(t)|\,. \tag{76}$$

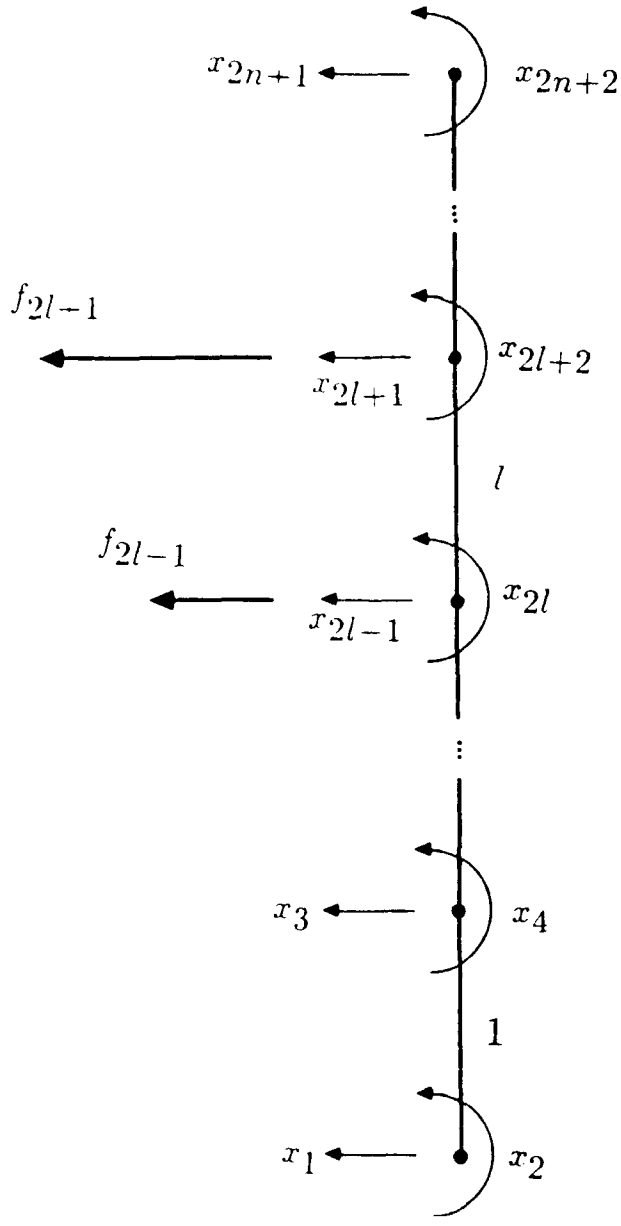

Figure 12: Global coordinate system for marine riser analysis.

Assuming k_D is not a function of the random vector, the derivative of Equation 75 with respect to b_i and evaluated at $\bar{\boldsymbol{b}}$ is

$$\left.\frac{\partial f_{D_{2l+1}}(t)}{\partial b_i}\right|_{\bar{\boldsymbol{b}}} = -2k_D \left|u_{2l+1}(t) - \dot{x}_{2l+1}(t)\right| \left.\frac{\partial \dot{x}_{2l+1}(t)}{\partial b_i}\right|_{\bar{\boldsymbol{b}}}. \tag{77}$$

A similar expression can also be developed for differentiating Equation 76 and is shown to be

$$\left.\frac{\partial f_{D_{2l-1}}(t)}{\partial b_i}\right|_{\bar{\boldsymbol{b}}} = -2k_D \left|u_{2l-1}(t) - \dot{x}_{2l-1}(t)\right| \left.\frac{\partial \dot{x}_{2l-1}(t)}{\partial b_i}\right|_{\bar{\boldsymbol{b}}}. \tag{78}$$

Note that first-order differentials of the hydrodynamic drag force terms are functions of the sensitivity of the structural velocity with respect to the elements of the random vector. It can be shown that the derivatives of the global drag force vector, $\left.\frac{\partial \boldsymbol{F}_c(t)}{\partial b_i}\right|_{\bar{\boldsymbol{b}}}$, can be expressed as the product of a matrix expression and the velocity sensitivity vectors. The element hydrodynamic drag force vector, $\tilde{F}_{D_l}(t)$, can be obtained by substituting the appropriate drag force terms into Equation 59, and the vector can be written as

$$\tilde{F}_{D_l}(t) = \left\{ \begin{array}{c} \frac{\ell}{2} f_{0_l}(t) + 0.15\ell^2 f_l'(t) \\ \frac{\ell^2}{12} f_{0_l}(t) + \frac{\ell^3}{30} f_l'(t) \\ \frac{\ell}{2} f_{0_l}(t) + 0.35\ell^2 f_l'(t) \\ -\frac{\ell^2}{2} f_{0_l}(t) - \frac{\ell^3}{20} f_l'(t) \end{array} \right\}, \tag{79}$$

where the constant drag force per length is

$$f_{0_l}(t) = f_{D_{2l-1}}(t) \tag{80}$$

and the linear variation in the drag force per length is

$$f_l'(t) = \frac{f_{D_{2l+1}}(t) - f_{D_{2l-1}}(t)}{\ell}. \tag{81}$$

Substituting Equations 80 and 81 into Equation 79 yields the following expression for the element drag force vector

$$\tilde{F}_{D_l}(t) = \begin{Bmatrix} 0.35\ell f_{D_{2l-1}}(t) + 0.15\ell f_{D_{2l+1}}(t) \\ \frac{\ell^2}{20} f_{D_{2l-1}}(t) + \frac{\ell^2}{30} f_{D_{2l+1}}(t) \\ 0.15\ell f_{D_{2l-1}}(t) + 0.35\ell f_{D_{2l+1}}(t) \\ -\frac{\ell^2}{7.5} f_{D_{2l-1}}(t) - \frac{\ell^2}{20} f_{D_{2l+1}}(t) \end{Bmatrix}. \tag{82}$$

Differentiating Equation 82 with respect to b_i and evaluating the resulting equations at $\bar{\boldsymbol{b}}$ yields

$$\left.\frac{\partial \tilde{F}_{D_l}(t)}{\partial b_i}\right|_{\bar{\boldsymbol{b}}} = \begin{Bmatrix} 0.35\ell \left.\frac{\partial f_{D_{2l-1}}(t)}{\partial b_i}\right|_{\bar{\boldsymbol{b}}} + 0.15\ell \left.\frac{\partial f_{D_{2l+1}}(t)}{\partial b_i}\right|_{\bar{\boldsymbol{b}}} \\ \frac{\ell^2}{20} \left.\frac{\partial f_{D_{2l-1}}(t)}{\partial b_i}\right|_{\bar{\boldsymbol{b}}} + \frac{\ell^2}{30} \left.\frac{\partial f_{D_{2l+1}}(t)}{\partial b_i}\right|_{\bar{\boldsymbol{b}}} \\ 0.15\ell \left.\frac{\partial f_{D_{2l-1}}(t)}{\partial b_i}\right|_{\bar{\boldsymbol{b}}} + 0.35\ell \left.\frac{\partial f_{D_{2l+1}}(t)}{\partial b_i}\right|_{\bar{\boldsymbol{b}}} \\ -\frac{\ell^2}{7.5} \left.\frac{\partial f_{D_{2l-1}}(t)}{\partial b_i}\right|_{\bar{\boldsymbol{b}}} - \frac{\ell^2}{20} \left.\frac{\partial f_{D_{2l+1}}(t)}{\partial b_i}\right|_{\bar{\boldsymbol{b}}} \end{Bmatrix}. \tag{83}$$

The expressions for $\left.\frac{\partial f_{D_{2l+1}}(t)}{\partial b_i}\right|_{\bar{\boldsymbol{b}}}$ and $\left.\frac{\partial f_{D_{2l-1}}(t)}{\partial b_i}\right|_{\bar{\boldsymbol{b}}}$ in Equations 77 and 78 can be substituted into Equation 83 which gives the following expression

$$\left.\frac{\partial \tilde{F}_{D_l}(t)}{\partial b_i}\right|_{\bar{\boldsymbol{b}}} = -2k_D \begin{Bmatrix} 0.35\ell \left|u_{2l-1}(t) - \dot{x}_{2l-1}(t)\right| \left.\frac{\partial \dot{x}_{2l-1}(t)}{\partial b_i}\right|_{\bar{\boldsymbol{b}}} \\ +0.15\ell \left|u_{2l+1}(t) - \dot{x}_{2l+1}(t)\right| \left.\frac{\partial \dot{x}_{2l+1}(t)}{\partial b_i}\right|_{\bar{\boldsymbol{b}}} \\ \frac{\ell^2}{20} \left|u_{2l-1}(t) - \dot{x}_{2l-1}(t)\right| \left.\frac{\partial \dot{x}_{2l-1}(t)}{\partial b_i}\right|_{\bar{\boldsymbol{b}}} \\ +\frac{\ell^2}{30} \left|u_{2l+1}(t) - \dot{x}_{2l+1}(t)\right| \left.\frac{\partial \dot{x}_{2l+1}(t)}{\partial b_i}\right|_{\bar{\boldsymbol{b}}} \\ 0.15\ell \left|u_{2l-1}(t) - \dot{x}_{2l-1}(t)\right| \left.\frac{\partial \dot{x}_{2l-1}(t)}{\partial b_i}\right|_{\bar{\boldsymbol{b}}} \\ +0.35\ell \left|u_{2l+1}(t) - \dot{x}_{2l+1}(t)\right| \left.\frac{\partial \dot{x}_{2l+1}(t)}{\partial b_i}\right|_{\bar{\boldsymbol{b}}} \\ -\frac{\ell^2}{7.5} \left|u_{2l-1}(t) - \dot{x}_{2l-1}(t)\right| \left.\frac{\partial \dot{x}_{2l-1}(t)}{\partial b_i}\right|_{\bar{\boldsymbol{b}}} \\ -\frac{\ell^2}{20} \left|u_{2l+1}(t) - \dot{x}_{2l+1}(t)\right| \left.\frac{\partial \dot{x}_{2l+1}(t)}{\partial b_i}\right|_{\bar{\boldsymbol{b}}} \end{Bmatrix}. \tag{84}$$

The sensitivity expressions for the velocity terms can be separated out of Equation 84 resulting in a new expression for $\left.\frac{\partial \tilde{F}_{D_l}(t)}{\partial b_i}\right|_{\bar{\boldsymbol{b}}}$ which can be written as

$$\left.\frac{\partial \tilde{F}_{D_l}(t)}{\partial b_i}\right|_{\bar{\boldsymbol{b}}} = -2k_D[R_l](t) \begin{Bmatrix} \left.\frac{\partial \dot{x}_{2l-1}(t)}{\partial b_i}\right|_{\bar{\boldsymbol{b}}} \\ \left.\frac{\partial \dot{x}_{2l}(t)}{\partial b_i}\right|_{\bar{\boldsymbol{b}}} \\ \left.\frac{\partial \dot{x}_{2l+1}(t)}{\partial b_i}\right|_{\bar{\boldsymbol{b}}} \\ \left.\frac{\partial \dot{x}_{2l-2}(t)}{\partial b_i}\right|_{\bar{\boldsymbol{b}}} \end{Bmatrix}, \tag{85}$$

where the matrix $[R_l](t)$ represents the matrix

$$[R_l](t) = \begin{bmatrix} 0.35\ell\,|u_{2l-1}(t) - \dot{x}_{2l-1}(t)| & 0 & 0.15\ell\,|u_{2l+1}(t) - \dot{x}_{2l+1}(t)| & 0 \\ \frac{\ell^2}{20}\,|u_{2l-1}(t) - \dot{x}_{2l-1}(t)| & 0 & \frac{\ell^2}{30}\,|u_{2l+1}(t) - \dot{x}_{2l+1}(t)| & 0 \\ 0.15\ell\,|u_{2l-1}(t) - \dot{x}_{2l-1}(t)| & 0 & 0.35\ell\,|u_{2l+1}(t) - \dot{x}_{2l+1}(t)| & 0 \\ -\frac{\ell^2}{7.5}\,|u_{2l-1}(t) - \dot{x}_{2l-1}(t)| & 0 & \frac{\ell^2}{20}\,|u_{2l+1}(t) - \dot{x}_{2l+1}(t)| & 0 \end{bmatrix}. \tag{86}$$

Upon inspection of Equation 86, it can be shown that the element matrices, $[R_l](t)$, can be assembled into a global matrix, $\boldsymbol{R}(t)$, using the same assembly procedures as used for the mass and stiffness matrices. The expression for the global hydrodynamic force vector, differentiated with respect to b_i and evaluated at $\bar{\boldsymbol{b}}$ can now be written as

$$\left.\frac{\partial \boldsymbol{F}_D(t)}{\partial bi}\right|_{\bar{\boldsymbol{b}}} = -2k_D\boldsymbol{R}(t)\left.\frac{\partial \dot{\boldsymbol{x}}(t)}{\partial b_i}\right|_{\bar{\boldsymbol{b}}}. \tag{87}$$

In the first-order equations of motion, the 'damping force' was expressed as $\bar{\boldsymbol{C}}\left.\frac{\partial \dot{\boldsymbol{x}}(t)}{\partial b_i}\right|_{\bar{\boldsymbol{b}}}$. A new damping matrix $\bar{\boldsymbol{C}}'(t)$ is defined and is expressed as

$$\bar{\boldsymbol{C}}'(t) = \bar{\boldsymbol{C}} + 2k_D\boldsymbol{R}_i(t). \tag{88}$$

The first-order equations of motion now become

$$\bar{M}\left.\frac{\partial \ddot{\boldsymbol{x}}(t)}{\partial b_i}\right|_{\bar{\boldsymbol{b}}} + \bar{C}_i'(t)\left.\frac{\partial \dot{\boldsymbol{x}}(t)}{\partial b_i}\right|_{\bar{\boldsymbol{b}}} + \bar{K}\left.\frac{\partial \boldsymbol{x}(t)}{\partial b_i}\right|_{\bar{\boldsymbol{b}}} =$$

$$\left.\frac{\partial \boldsymbol{F}_c}{\partial b_i}\right|_{\bar{\boldsymbol{b}}} + \left.\frac{\partial \boldsymbol{F}_I(t)}{\partial b_i}\right|_{\bar{\boldsymbol{b}}} + \left.\frac{\partial \boldsymbol{F}_c(t)}{\partial b_i}\right|_{\bar{\boldsymbol{b}}} - \left[\left.\frac{\partial \boldsymbol{M}}{\partial b_i}\right|_{\bar{\boldsymbol{b}}}\ddot{\bar{\boldsymbol{x}}}(t) + \left.\frac{\partial \boldsymbol{C}}{\partial b_i}\right|_{\bar{\boldsymbol{b}}}\dot{\bar{\boldsymbol{x}}}(t) + \left.\frac{\partial \boldsymbol{K}}{\partial b_i}\right|_{\bar{\boldsymbol{b}}}\bar{\boldsymbol{x}}(t)\right], \quad (89)$$

Note that the static and dynamic components in Equation 89 must be separated to be consistent with the prescribed solution procedure. Thus, the sensitivity vectors obtained by solving the static first-order equation include the static offset sensitivity vectors, $\left.\frac{\partial \boldsymbol{x}_s}{\partial b_i}\right|_{\bar{\boldsymbol{b}}}$, and the sensitivity kinematic vectors computed by solving the dynamic first-order equations. These include the dynamic response, velocity and acceleration sensitivity vectors, $\left.\frac{\partial \boldsymbol{x}_d(t)}{\partial b_i}\right|_{\bar{\boldsymbol{b}}}$, $\left.\frac{\partial \dot{\boldsymbol{x}}_d(t)}{\partial b_i}\right|_{\bar{\boldsymbol{b}}}$, and $\left.\frac{\partial \ddot{\boldsymbol{x}}_d(t)}{\partial b_i}\right|_{\bar{\boldsymbol{b}}}$, respectively.

4.3.3 Second-Order Response Predictions

Once the sensitivity vectors have been computed, the second-order deviations about the zeroeth-order response predictions can be obtained. These predictions require second-order partial differentiation of the system matrices and force vectors with respect to b_i and b_j, where the resulting expressions are evaluated at $\bar{\boldsymbol{b}}$. It is not difficult to obtain expressions for $\left.\frac{\partial^2 \boldsymbol{M}}{\partial b_i \partial b_j}\right|_{\bar{\boldsymbol{b}}}$, $\left.\frac{\partial^2 \boldsymbol{C}}{\partial b_i \partial b_j}\right|_{\bar{\boldsymbol{b}}}$, $\left.\frac{\partial^2 \boldsymbol{K}}{\partial b_i \partial b_j}\right|_{\bar{\boldsymbol{b}}}$, $\left.\frac{\partial^2 \boldsymbol{F}_c}{\partial b_i \partial b_j}\right|_{\bar{\boldsymbol{b}}}$, $\left.\frac{\partial^2 \boldsymbol{F}_I(t)}{\partial b_i \partial b_j}\right|_{\bar{\boldsymbol{b}}}$ and $\left.\frac{\partial^2 \boldsymbol{F}_c(t)}{\partial b_i \partial b_j}\right|_{\bar{\boldsymbol{b}}}$. However, obtaining the solution for $\left.\frac{\partial^2 \boldsymbol{F}_c(t)}{\partial b_i \partial b_j}\right|_{\bar{\boldsymbol{b}}}$ is complicated.

The second-order derivative of the hydrodynamic force per length at the top of element l is obtained by differentiating Equation 75 with respect to b_i and b_j and evaluating the resulting expression at $\bar{\boldsymbol{b}}$. This can be expressed as

$$\left.\frac{\partial^2 f_{D_{2l+1}}(t)}{\partial b_i \partial b_j}\right|_{\bar{\boldsymbol{b}}} = -2k_D\,|u_{2l+1}(t) - \dot{x}_{2l+1}(t)|\left.\frac{\partial^2 \dot{x}_{2l+1}(t)}{\partial b_i \partial b_j}\right|_{\bar{\boldsymbol{b}}}$$

$$+ 2k_D\,\mathrm{sgn}[u_{2l+1}(t) - \dot{x}_{2l+1}(t)]\left.\frac{\partial \dot{x}_{2l+1}(t)}{\partial b_i}\right|_{\bar{\boldsymbol{b}}}\left.\frac{\partial \dot{x}_{2l+1}(t)}{\partial b_j}\right|_{\bar{\boldsymbol{b}}}. \quad (90)$$

At the bottom of element l this expression becomes

$$\left.\frac{\partial^2 f_{D_{2l-1}}(t)}{\partial b_i \partial b_j}\right|_{\bar{\boldsymbol{b}}} = -2k_D \left|u_{2l-1}(t) - \dot{x}_{2l-1}(t)\right| \left.\frac{\partial^2 \dot{x}_{2l-1}(t)}{\partial b_i \partial b_j}\right|_{\bar{\boldsymbol{b}}}$$

$$+ 2k_D \,\mathrm{sgn}[u_{2l-1}(t) - \dot{x}_{2l-1}(t)] \left.\frac{\partial \dot{x}_{2l-1}(t)}{\partial b_i}\right|_{\bar{\boldsymbol{b}}} \left.\frac{\partial \dot{x}_{2l-1}(t)}{\partial b_j}\right|_{\bar{\boldsymbol{b}}}, \tag{91}$$

where for an arbitrary function, g, the operator sgn$[g]$ is defined as

$$\mathrm{sgn}[g] = \begin{cases} 1 & \text{for } g > 0 \\ -1 & \text{for } g < 0 \\ \text{undefined} & \text{at } g = 0 \end{cases}. \tag{92}$$

Note that in the event that the relative velocity between the wave and structure is zero, the sgn operator is undefined. The second-order differential of the drag force vector is not a continuous function when the relative velocity is zero, and can be shown to have two values which are equal and opposite in sign. For the purpose of numerical simulation, when the relative velocity is equal to zero, the operator sgn[0] is defined as zero. Thus, the second-order derivative of the drag force is defined as zero.

An expression for the second-order partial derivatives of the element hydrodynamic drag force vector with respect to b_i and b_j and evaluated at $\bar{\boldsymbol{b}}$ can be obtained using an approach similar to the one used to derive the first-order expression. The final expression for the second-order partial derivative of the lth element of the hydrodynamic force vector with respect to b_i and b_j and evaluated at $\bar{\boldsymbol{b}}$ is

$$\left.\frac{\partial^2 \tilde{F}_{D_l}(t)}{\partial b_i \partial b_j}\right|_{\bar{\boldsymbol{b}}} = -2k_D[R_l](t) \begin{Bmatrix} \left.\frac{\partial^2 \dot{x}_{2l-1}(t)}{\partial b_i \partial b_j}\right|_{\bar{\boldsymbol{b}}} \\ \left.\frac{\partial^2 \dot{x}_{2l}(t)}{\partial b_i \partial b_j}\right|_{\bar{\boldsymbol{b}}} \\ \left.\frac{\partial^2 \dot{x}_{2l+1}(t)}{\partial b_i \partial b_j}\right|_{\bar{\boldsymbol{b}}} \\ \left.\frac{\partial^2 \dot{x}_{2l-2}(t)}{\partial b_i \partial b_j}\right|_{\bar{\boldsymbol{b}}} \end{Bmatrix}$$

$$+ 2k_D[R_l'](t) \begin{Bmatrix} \frac{\partial \dot{x}_{2l-1}(t)}{\partial b_i}\Big|_{\bar{\boldsymbol{b}}} & \frac{\partial \dot{x}_{2l-1}(t)}{\partial b_j}\Big|_{\bar{\boldsymbol{b}}} \\ 0 \\ \frac{\partial \dot{x}_{2l+1}(t)}{\partial b_i}\Big|_{\bar{\boldsymbol{b}}} & \frac{\partial \dot{x}_{2l+1}(t)}{\partial b_j}\Big|_{\bar{\boldsymbol{b}}} \\ 0 \end{Bmatrix}, \tag{93}$$

where $[R_l'](t)$ is defined by the matrix expression

$$[R_l'](t) = \begin{bmatrix} 0.35\ell\,\mathrm{sgn}[u_{2l-1}(t) - \dot{x}_{2l-1}(t)] & 0 & 0.15\ell\,\mathrm{sgn}[u_{2l+1}(t) - \dot{x}_{2l+1}(t)] & 0 \\ \frac{\ell^2}{20}\,\mathrm{sgn}[u_{2l-1}(t) - \dot{x}_{2l-1}(t)] & 0 & \frac{\ell^2}{30}\,\mathrm{sgn}[u_{2l+1}(t) - \dot{x}_{2l+1}(t)] & 0 \\ 0.15\ell\,\mathrm{sgn}[u_{2l-1}(t) - \dot{x}_{2l-1}(t)] & 0 & 0.35\ell\,\mathrm{sgn}[u_{2l+1}(t) - \dot{x}_{2l+1}(t)] & 0 \\ -\frac{\ell^2}{7.5}\,\mathrm{sgn}[u_{2l-1}(t) - \dot{x}_{2l-1}(t)] & 0 & -\frac{\ell^2}{20}\,\mathrm{sgn}[u_{2l+1}(t) - \dot{x}_{2l+1}(t)] & 0 \end{bmatrix}. \tag{94}$$

The global matrices, $\boldsymbol{R}(t)$ and $\boldsymbol{R}'(t)$ can be assembled using the same assembly procedure as for the mass and stiffness matrices. The second-order partial derivatives of the global hydrodynamic drag force vector with respect to b_i and b_j and evaluated at $\bar{\boldsymbol{b}}$ can now be expressed as

$$\frac{\partial^2 \boldsymbol{F}_D(t)}{\partial b_i \partial b_j}\Big|_{\bar{\boldsymbol{b}}} = -2k_D \boldsymbol{R}(t)\, \frac{\partial^2 \dot{\boldsymbol{x}}(t)}{\partial b_i \partial b_j}\Big|_{\bar{\boldsymbol{b}}} + 2k_D \boldsymbol{R}'(t)\dot{\boldsymbol{x}}'(t), \tag{95}$$

where for an n-degree of freedom system $\dot{\boldsymbol{x}}'(t)$ can be written as

$$\dot{\boldsymbol{x}}'(t) = \left\{ \begin{array}{c} \left.\frac{\partial \dot{x}_1(t)}{\partial b_i}\right|_{\bar{\boldsymbol{b}}} \left.\frac{\partial \dot{x}_1(t)}{\partial b_j}\right|_{\bar{\boldsymbol{b}}} \\ 0 \\ \left.\frac{\partial \dot{x}_3(t)}{\partial b_i}\right|_{\bar{\boldsymbol{b}}} \left.\frac{\partial \dot{x}_3(t)}{\partial b_j}\right|_{\bar{\boldsymbol{b}}} \\ 0 \\ \vdots \\ \left.\frac{\partial \dot{x}_{n-3}(t)}{\partial b_i}\right|_{\bar{\boldsymbol{b}}} \left.\frac{\partial \dot{x}_{n-3}(t)}{\partial b_j}\right|_{\bar{\boldsymbol{b}}} \\ 0 \\ \left.\frac{\partial \dot{x}_{n-1}(t)}{\partial b_i}\right|_{\bar{\boldsymbol{b}}} \left.\frac{\partial \dot{x}_{n-1}(t)}{\partial b_j}\right|_{\bar{\boldsymbol{b}}} \\ 0 \end{array} \right\}. \tag{96}$$

Recall that the second-order equation of motion as developed in Chapter 2 was shown to be

$$\bar{\boldsymbol{M}}\Delta\ddot{\bar{\boldsymbol{x}}}(t) + \bar{\boldsymbol{C}}\Delta\dot{\bar{\boldsymbol{x}}}(t) + \bar{\boldsymbol{K}}\Delta\bar{\boldsymbol{x}}(t) = \Delta\hat{\boldsymbol{F}}(t), \tag{97}$$

where

$$\Delta\hat{\boldsymbol{F}}(t) = \frac{1}{2}\sum_{i=1}^{q}\sum_{j=1}^{q}\left\{\left.\frac{\partial^2 \boldsymbol{F}(t)}{\partial b_i \partial b_j}\right|_{\bar{\boldsymbol{b}}} \mathrm{Cov}[b_i, b_j]\right\}$$

$$-\sum_{i=1}^{q}\sum_{j=1}^{q}\left\{\left[\left.\frac{\partial \boldsymbol{M}}{\partial b_i}\right|_{\bar{\boldsymbol{b}}} \left.\frac{\partial \ddot{\boldsymbol{x}}(t)}{\partial b_j}\right|_{\bar{\boldsymbol{b}}} + \left.\frac{\partial \boldsymbol{C}}{\partial b_i}\right|_{\bar{\boldsymbol{b}}} \left.\frac{\partial \dot{\boldsymbol{x}}(t)}{\partial b_j}\right|_{\bar{\boldsymbol{b}}} + \left.\frac{\partial \boldsymbol{K}}{\partial b_i}\right|_{\bar{\boldsymbol{b}}} \left.\frac{\partial \boldsymbol{x}(t)}{\partial b_j}\right|_{\bar{\boldsymbol{b}}}\right] \mathrm{Cov}[b_i, b_j]\right\}$$

$$-\frac{1}{2}\sum_{i=1}^{q}\sum_{j=1}^{q}\left\{\left[\left.\frac{\partial^2 \boldsymbol{M}}{\partial b_i \partial b_j}\right|_{\bar{\boldsymbol{b}}} \ddot{\bar{\boldsymbol{x}}}(t) + \left.\frac{\partial^2 \boldsymbol{C}}{\partial b_i \partial b_j}\right|_{\bar{\boldsymbol{b}}} \dot{\bar{\boldsymbol{x}}}(t) + \left.\frac{\partial^2 \boldsymbol{K}}{\partial b_i \partial b_j}\right|_{\bar{\boldsymbol{b}}} \bar{\boldsymbol{x}}(t)\right] \mathrm{Cov}[b_i, b_j]\right\}. \tag{98}$$

Upon substitution of Equation 95 into the second-order equation, the second-order deviation about the mean drag force vector can be expressed as

$$\frac{1}{2}\sum_{i=1}^{q}\sum_{j=1}^{q}\left\{\left.\frac{\partial^2 \boldsymbol{F}_D(t)}{\partial b_i \partial b_j}\right|_{\bar{\boldsymbol{b}}} \mathrm{Cov}[b_i, b_j]\right\} = -2k_D \boldsymbol{R}(t)\frac{1}{2}\sum_{i=1}^{q}\sum_{j=1}^{q}\left\{\left.\frac{\partial^2 \dot{\boldsymbol{x}}(t)}{\partial b_i \partial b_j}\right|_{\bar{\boldsymbol{b}}} \mathrm{Cov}[b_i, b_j]\right\}$$

$$+ 2k_D \boldsymbol{R}'(t) \frac{1}{2} \sum_{i=1}^{q} \sum_{j=1}^{q} \left\{ \dot{\boldsymbol{x}}'(t) \mathrm{Cov}[b_i, b_j] \right\}. \tag{99}$$

The form of this equation can be simplified, where the new equation is

$$\frac{1}{2} \sum_{i=1}^{q} \sum_{j=1}^{q} \left\{ \left. \frac{\partial^2 \boldsymbol{F}_D(t)}{\partial b_i \partial b_j} \right|_{\bar{\boldsymbol{b}}} \mathrm{Cov}[b_i, b_j] \right\} = -2k_D \boldsymbol{R}(t) \Delta \bar{\boldsymbol{x}}(t)$$

$$+ 2k_D \boldsymbol{R}'(t) \frac{1}{2} \sum_{i=1}^{q} \sum_{j=1}^{q} \left\{ \dot{\boldsymbol{x}}'(t) \mathrm{Cov}[b_i, b_j] \right\}. \tag{100}$$

The second–order equation of motion can now be expressed as

$$\bar{\boldsymbol{M}} \Delta \ddot{\bar{\boldsymbol{x}}}(t) + \bar{\boldsymbol{C}}'(t) \Delta \dot{\bar{\boldsymbol{x}}}(t) + \bar{\boldsymbol{K}} \Delta \bar{\boldsymbol{x}}(t) =$$

$$\Delta \hat{\boldsymbol{F}}(t) + 2k_D \boldsymbol{R}'(t) \frac{1}{2} \sum_{i=1}^{q} \sum_{j=1}^{q} \left\{ \dot{\boldsymbol{x}}'(t) \mathrm{Cov}[b_i, b_j] \right\} \tag{101}$$

where

$$\Delta \hat{\boldsymbol{F}}(t) = \frac{1}{2} \sum_{i=1}^{q} \sum_{j=1}^{q} \left\{ \left. \frac{\partial^2 (\boldsymbol{F}_I(t) + \boldsymbol{F}_c + \boldsymbol{F}_e(t))}{\partial b_i \partial b_j} \right|_{\bar{\boldsymbol{b}}} \mathrm{Cov}[b_i, b_j] \right\}$$

$$- \sum_{i=1}^{q} \sum_{j=1}^{q} \left\{ \left[\left. \frac{\partial \boldsymbol{M}}{\partial b_i} \right|_{\bar{\boldsymbol{b}}} \left. \frac{\partial \ddot{\boldsymbol{x}}(t)}{\partial b_j} \right|_{\bar{\boldsymbol{b}}} + \left. \frac{\partial \boldsymbol{C}}{\partial b_i} \right|_{\bar{\boldsymbol{b}}} \left. \frac{\partial \dot{\boldsymbol{x}}(t)}{\partial b_j} \right|_{\bar{\boldsymbol{b}}} + \left. \frac{\partial \boldsymbol{K}}{\partial b_i} \right|_{\bar{\boldsymbol{b}}} \left. \frac{\partial \boldsymbol{x}(t)}{\partial b_j} \right|_{\bar{\boldsymbol{b}}} \right] \mathrm{Cov}[b_i, b_j] \right\}$$

$$- \frac{1}{2} \sum_{i=1}^{q} \sum_{j=1}^{q} \left\{ \left[\left. \frac{\partial^2 \boldsymbol{M}}{\partial b_i \partial b_j} \right|_{\bar{\boldsymbol{b}}} \ddot{\bar{\boldsymbol{x}}}(t) + \left. \frac{\partial^2 \boldsymbol{C}}{\partial b_i \partial b_j} \right|_{\bar{\boldsymbol{b}}} \dot{\bar{\boldsymbol{x}}}(t) + \left. \frac{\partial^2 \boldsymbol{K}}{\partial b_i \partial b_j} \right|_{\bar{\boldsymbol{b}}} \bar{\boldsymbol{x}}(t) \right] \mathrm{Cov}[b_i, b_j] \right\}. \tag{102}$$

Note that the static and dynamic components in Equation 102 must be separated to be consistent with the prescribed solution procedure. The second–order deviations in the static offset vector are obtained by solving the second–order equation with only the static components, and the second–order static response is written as $\Delta \bar{\boldsymbol{x}}_s$. The second–order deviations in the dynamic response, $\Delta \bar{\boldsymbol{x}}_d(t)$ are computed by solving Equation 101 using only those components which contribute to the dynamic response. The total expected response of the riser accurate to second–order can now be written as

$$\mathrm{E}[\boldsymbol{x}(t)] = \bar{\boldsymbol{x}}_s + \Delta \bar{\boldsymbol{x}}_s + \bar{\boldsymbol{x}}_d(t) + \Delta \bar{\boldsymbol{x}}_d(t). \tag{103}$$

A better approximation for the expected values in the stresses can be obtained by substituting the appropriate second-order accurate expected values of the rotations into Equation 73.

4.3.4 First-Order Accurate Covariance Predictions

The covariances for the discrete displacement fields can be computed as described in Chapter 2. The covariance between any two displacements $x_l(t)$ and $x_m(t)$ at time t are computed from the following formula

$$\mathrm{Cov}[x_l(t), x_m(t)] \approx$$

$$\sum_{i=1}^{q}\sum_{j=1}^{q}\left\{\left(\left.\frac{\partial(x_{s_l}+x_{d_l}(t))}{\partial b_i}\right|_{\bar{\boldsymbol{b}}}\right)\left(\left.\frac{\partial(x_{s_m}+x_{d_m}(t))}{\partial b_j}\right|_{\bar{\boldsymbol{b}}}\right)\mathrm{Cov}[b_i,b_j]\right\}. \tag{104}$$

One method for obtaining the covariances in the stress field is to employ the second-moment analysis techniques. The first-order equation is obtained by differentiating both sides of Equation 72 with respect to each of the elements in the random vector and evaluating the resulting expressions at the expected values of the random vector. Thus, the first-order equation for the stress at the midpoint of element l at time t, assuming E and c are deterministic, can be expressed as

$$\left.\frac{\partial\sigma_l(t)}{\partial b_i}\right|_{\bar{\boldsymbol{b}}} \approx \frac{Ec}{2\Delta z_l}\left\{\left.\frac{\partial\theta(z_l+\Delta z_l,t)}{\partial b_i}\right|_{\bar{\boldsymbol{b}}} - \left.\frac{\partial\theta(z_l-\Delta z_l,t)}{\partial b_i}\right|_{\bar{\boldsymbol{b}}}\right\}. \tag{105}$$

The first-order accurate covariance in the stresses at the midpoints of elements l and m are computed as

$$\mathrm{Cov}[\sigma_l(t), \sigma_m(t)] \approx$$

$$\sum_{i=1}^{q}\sum_{j=1}^{q}\left\{\left(\left.\frac{\partial\sigma_l(t)}{\partial b_i}\right|_{\bar{\boldsymbol{b}}}\right)\left(\left.\frac{\partial\sigma_m(t)}{\partial b_j}\right|_{\bar{\boldsymbol{b}}}\right)\mathrm{Cov}[b_i,b_j]\right\}. \tag{106}$$

In this study, only the variances in the stresses at the midpoint of the elements are required and a more direct method is used to compute these values. Squaring

both sides of Equation 72 and taking the expected value of the resulting expression yields

$$\mathrm{E}[(\sigma_l(t))^2] \approx \left(\frac{Ec}{2\Delta z_l}\right)^2 \mathrm{E}[\{\theta(z_l + \Delta z_l, t) - \theta(z_l - \Delta z_l, t)\}^2]. \qquad (107)$$

Equation 107 can be expanded, and assuming the means have been removed from the rotations, the variance in the stresses at the midpoint of element l and at time t can be computed as

$$\begin{aligned}\mathrm{var}[\sigma_l(t)] \approx \left(\frac{Ec}{2\Delta z_l}\right)^2 &\{\mathrm{var}[\theta(z_l + \Delta z_l, t)] + \mathrm{var}[\theta(z_l - \Delta z_l, t)]\} \\ &- 2\left(\frac{Ec}{2\Delta z_l}\right)^2 \{\mathrm{Cov}[\theta(z_l + \Delta z_l, t), \theta(z_l - \Delta z_l, t)]\}\,. \qquad (108)\end{aligned}$$

4.3.5 Application of Probabilistic Results

The probabilistic finite element results for the marine riser displacements and stresses can be used to assess the displacement and stress envelopes typically developed for design. The zeroeth–order solutions obtained in the probabilistic analysis would represent those obtained using a deterministic approach. The zeroeth–order displacement envelope can be estimated using the zeroeth–order displacement solutions. The stress envelope can also be developed where the stresses are predicted from the time histories of the zeroeth–order rotations.

Upper and lower bounds to the displacement and stress envelopes can also be computed. An upper bound time history for the displacements and stresses may be generated by adding the standard deviation to the zeroeth–order predicted values at time t. Similarly, a lower bound time history is created by subtracting the standard deviation from the time histories. Using these estimates for the maximum and minimum displacements and stresses at time t, upper and lower bounds for the displacement and stress envelopes can be estimated.

A better approximation for the displacement envelope is obtained using the second–order expected values of the responses. Similarly, a better approximation for the stress envelope is obtained using the stresses computed from the second–order rotations. These envelopes are then bounded as before. The upper bounds are computed from the sum of the second–order time histories and the first–order standard deviation time histories. The lower bounds are computed from the difference between the second–order time histories and the first–order standard deviation time histories.

4.4 Probabilistic Solutions to Marine Riser Problems

There are numerous commercial computer codes available for the analysis of marine riser systems. In an attempt to compare the predictive capabilities of the offshore industry, the American Petroleum Institute (API), posed a set of standard problems to which it solicited industry solutions. API then prepared a bulletin based upon the numerical results it received (API 1977). The bulletin contains predictions for riser systems designed for 500, 1500 and 3000 feet of water. Since all the models require empirical data and the computer programs covered a wide range of solution techniques, the solutions were presented in terms of envelopes of displacement and stress.

The probabilistic finite element method, as developed in the preceding text, is used to predict the response behavior of marine riser systems which are considered to have random properties. Two marine riser systems are considered, the first in 500 feet of water and the second in 3000 feet of water. The riser system in 3000 feet of water includes external buoyant material. For each water depth the API bulletin shows a number of solutions submitted by the offshore industry in the form of response and stress envelopes. For the purpose of comparison, the

solutions shown in the API bulletin are presented on the appropriate graphs in this study. The mean values of the parameters which are necessary to perform the analyses are specified in the API bulletin and are tabulated in Table 2. The probabilistic solutions are compared with results obtained in an API bulletin on marine riser analyses. Monte Carlo simulations are also performed as a means of assessing the probabilistic results.

To be consistent with the results in the API bulletin and to show results which are meaningful to engineers who design marine risers, response and stress envelopes are generated and bounded by one standard deviation. Zeroeth–order predictions which are analogous to the deterministic solutions predicted in the API bulletin are shown, as are the second–order approximations. The standard deviations in the response parameters are obtained by taking the root of the first–order accurate variance. The bounds to the displacement and stress envelopes computed in this study are obtained by bounding the appropriate time series with one standard deviation computed at time t, and then computing the envelopes for these solutions.

The finite element riser models are assembled using twenty–four elements and fifty degrees of freedom. The models are assembled such that the individual elements are concentrated in the regions where the maximum stresses are expected to occur. These regions are dictated by the imposed boundary conditions and are located near the top and bottom of the risers. The element lengths for the 500 foot water depth case range from 10 to 30 feet and the element lengths for the 3000 foot water depth case range from 20 feet to 200 feet.

Table 2: Riser input data specifications.

A. Constant with water depth	
Riser data	
Diameters, inches	
riser pipe outside diameter	16.0
riser pipe inside diameter	14.75
choke line outside diameter	4.0
choke line inside diameter	2.7
kill line outside diameter	4.0
kill line outside diameter	2.7
buoyant material outside diameter	24.0
Modulus of elasticity of pipe, psi $\times 10^6$	30
Densities, pounds/cubic foot	
sea water	64
drilling mud	89.8
Hydraulic force constants	
drag coefficient	0.7
added mass coefficient	1.5
effective diameter, inches	26
Weight (*includes mud in external lines*), pounds / foot	
unbuoyed	172.4
buoyed	188.1
Linear current profile:	
velocity at the surface, knots	0.5
velocity at the lower ball joint, knots	0
Vertical distances, feet	
mean water level to riser support ring	50
sea floor to lower ball joint	
B. Varying with water depth	
Top tension, kips	
500 foot water depth	120
3000 foot water depth	500
Static offset, 3% of water depth	
C. Dynamic	
wave height, feet	20
wave period, seconds	9
vessel surge amplitude, feet	2
phase lag between vessel and wave, degrees	15

4.4.1 Top Tension Modeled as a Random Variable

To demonstrate the predictive capability of the probabilistic finite element method, two marine riser systems are examined in which the tension applied to the top of the risers is considered to fluctuate. The water depths considered are 500 and 3000 feet and the properties of the risers are given in Table 2. The distributions of the random top tensions are considered to be Gaussian and the coefficient of variation in the top tension for both cases is assumed to be 0.1.

Monte Carlo simulations are performed to assess the second-moment results. The Monte Carlo technique is identical to the one used in the Chapter 3. It was determined that the second-moment solutions converge within 400 simulations.

Figures 13 and 14 show the maximum steady state response predicted by the zeroeth- and second-order solutions and the Monte Carlo solutions for the 500 foot and 3000 foot water depth cases, respectively. For each response estimate, one standard deviation in response is added. Thus the lower curve represents the response estimate and the upper curve represents a possible 'upper bound' to the estimate. The API response predictions are also shown. As expected, the zeroeth-order solution falls within the bounds of the API solutions. There is some deviation in the zeroeth-order solutions and those predicted using the Monte Carlo simulation. The second-order solutions do converge to those predicted from the Monte Carlo simulations. It should be noted that when one standard deviation in response, predicted using second-moment techniques or by the Monte Carlo simulation, is added to the appropriate mean response prediction, the upper bound of the API solutions is exceeded.

Figure 15 represents the minimum steady state response for the riser in 500 feet of water. The second-order solutions converge to those predicted in the Monte

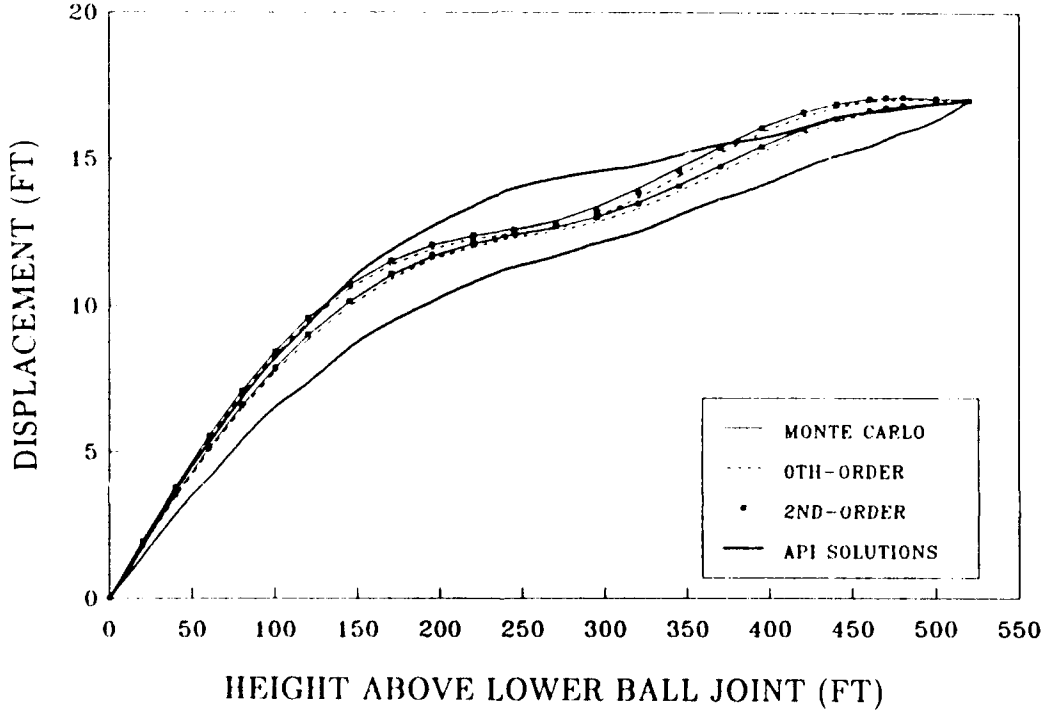

Figure 13: Maximum displacement and bounds for riser with random top tension in 500 feet of water.

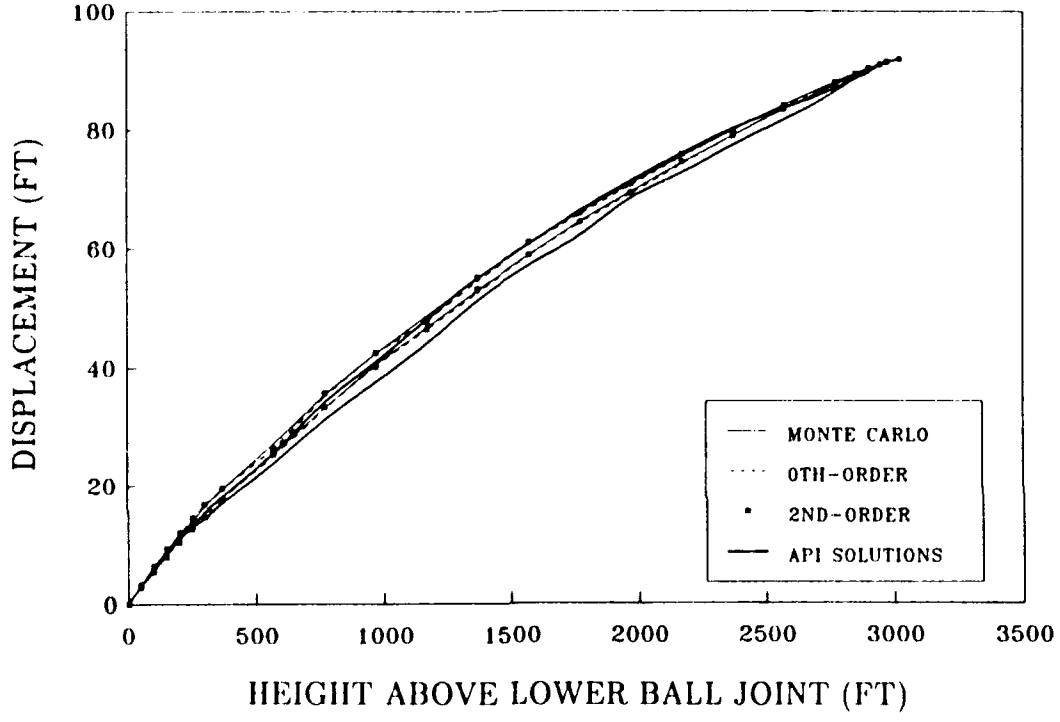

Figure 14: Maximum displacement and bounds for riser with random top tension in 3000 feet of water.

Carlo simulation, where these solutions are slightly different from the zeroeth-order solution. The lower set of response curves represent the response predictions minus one standard deviation and are shown to fall outside of the bounds of the response predictions given in the API bulletin.

Figure 16 compares the standard deviations associated with the maximum and minimum steady state response of the riser in 3000 feet of water, where the first-order accurate predictions are compared with those obtained using the Monte Carlo method. For illustrative purposes the bottom curve represents the standard deviation which was subtracted from the minimum response and is multiplied by the factor -1. The first-order solution appears to be similar to the Monte Carlo solution, but at some depths the first-order solution overshoots and undershoots the standard deviations predicted from the Monte Carlo simulation. It was noted from the time series of the standard deviations that there is some overshoot of the Monte Carlo solutions by the first-order predictions, as explained by the resonant effects. However, this is generally small due to the large amount of hydrodynamic damping.

Figures 17 and 18 indicate the stress envelopes predicted by the zeroeth- and second-order solutions and the Monte Carlo simulations for the 500 and 3000 foot water depth cases, respectively. For the 500 foot water depth case the zeroeth-order solutions are different than the Monte Carlo solutions and the second-order solutions converge to those predicted using the Monte Carlo technique. For the 3000 foot water depth case the second-order solution does not converge to the Monte Carlo prediction for the peak stresses near the bottom of the riser. Perhaps the reason the second-order solution does not converge is related to the number and spacing of the elements. The number of elements used for this case was the same as for the 500 foot case, where the elements were spaced closest in the areas

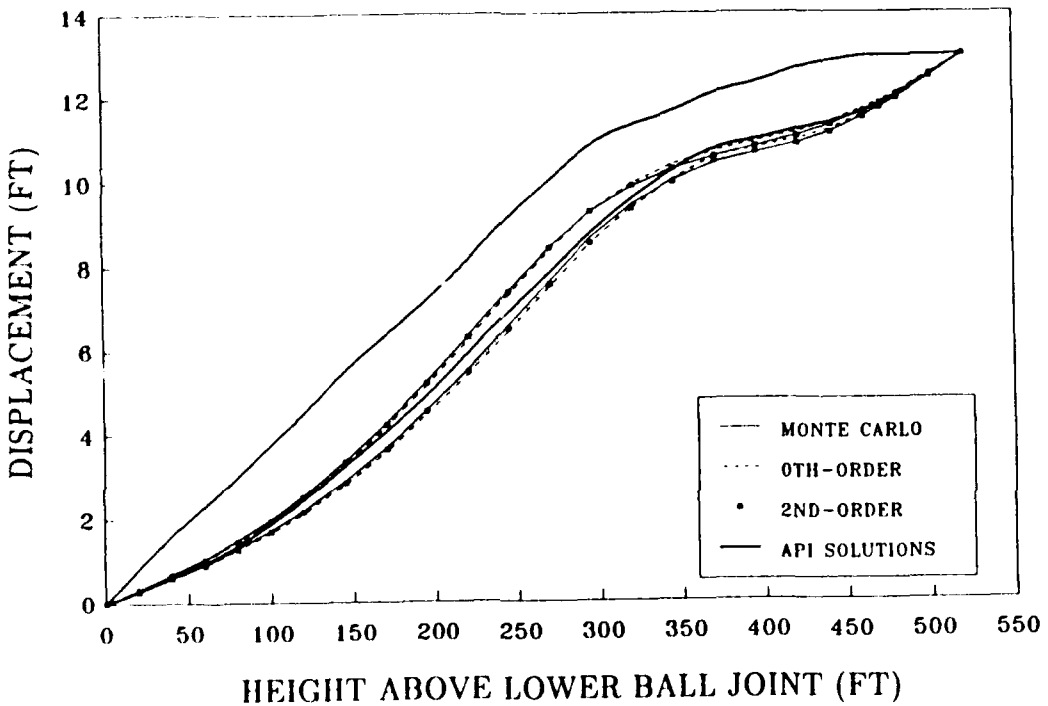

Figure 15: Minimum displacement and bounds for riser with random top tension in 500 feet of water.

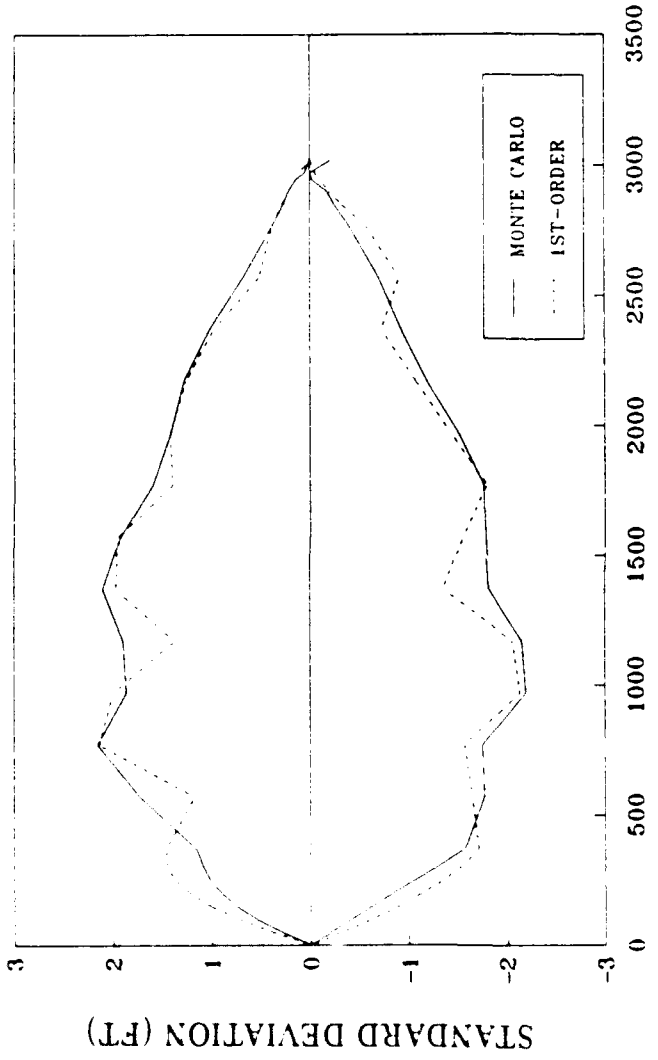

Figure 16: Standard deviations to be added to zeroeth order and Monte Carlo response envelopes for riser in 3000 feet of water.

where the maximum stresses were expected to occur. In this study the maximum number of elements permitted for higher-order response predictions was twenty-four. Both the zeroeth- and second-order predictions of the maximum stress at the top of the riser converge to the Monte Carlo results.

Figures 19 and 20 indicate the maximum zeroeth- and second-order stresses and those predicted using the Monte Carlo simulations for the 500 and 3000 foot water depth case, respectively. The upper set of curves represents one standard deviation in addition to the value of the mean estimate. The bounds from the API solutions are also shown. For the 500 foot water depth case it is seen that the second-order solutions converge to Monte Carlo solutions. Note that the peak stress predicted from the zeroeth-order solution lies within the bounds of the API solutions and that the second-order and Monte Carlo solutions are outside the bounds. Further, note that with the addition of one standard deviation to mean stresses, the probabilistic estimates can exceed the estimates obtained in conventional analyses by a significant amount. For the 3000 foot case where the variation in the stresses is much smaller than for the 500 foot case, the predictions appear to be within the range of the API solutions.

4.4.2 Unit Weight of Drilling Mud Modeled as a Random Field

To further demonstrate the possibilities for simulation using probabilistic finite element methods, another type of marine riser simulation is presented. In this case a riser system in 500 feet of water, as specified in Table 2, is examined assuming that the unit weight of the drilling mud varies along the riser according to a definable statistical process. A first-order autoregressive model, AR(1), is used to account for the fluctuations. Accordingly, the fluctuations in the weight per unit length of the drilling mud, $\bar{w}_m(z)$ at an elevation z, above the sea floor

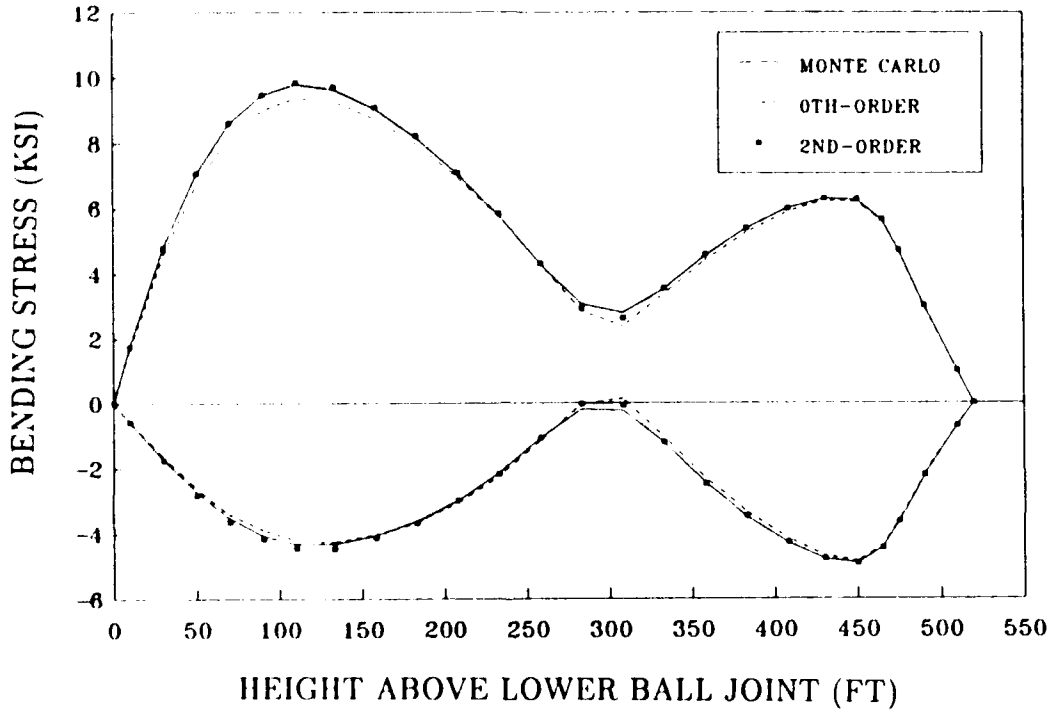

Figure 17: Bending stress envelopes for riser with random top tension in 500 feet of water.

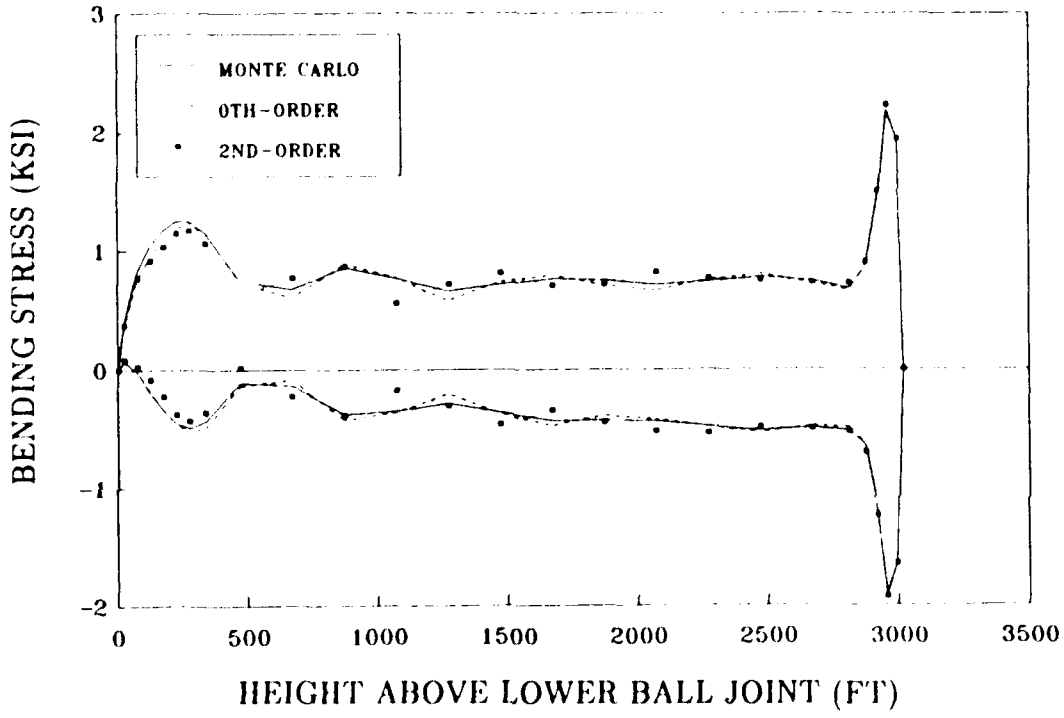

Figure 18: Bending stress envelopes for riser with random top tension in 3000 feet of water.

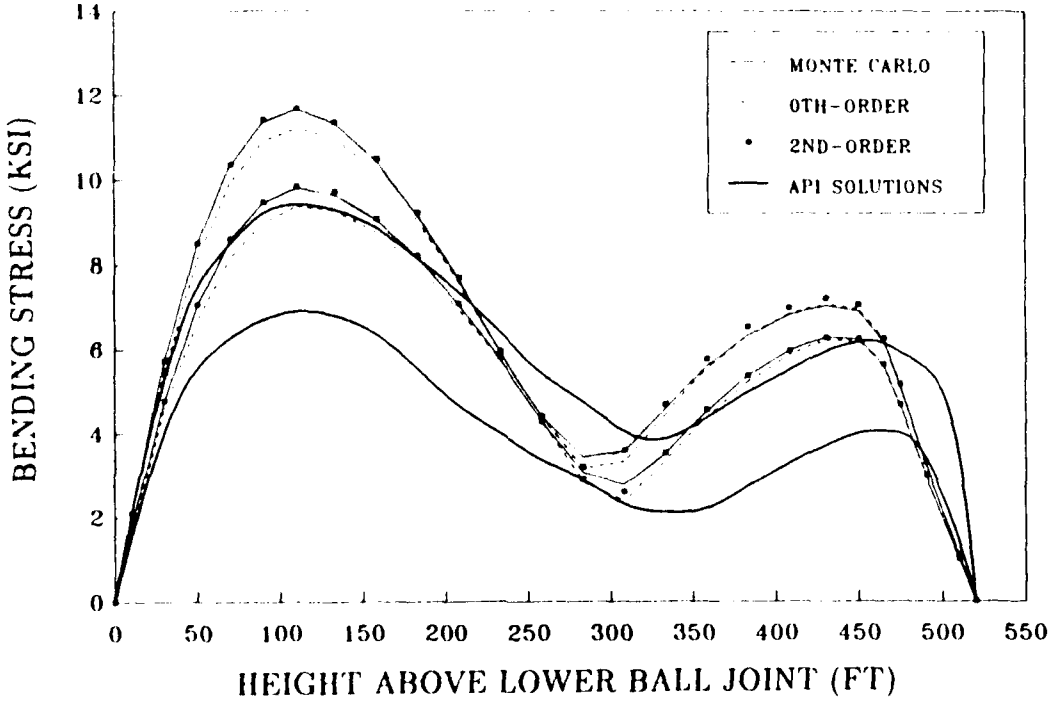

Figure 19: Maximum bending stress and bounds for riser with random top tension in 500 feet of water.

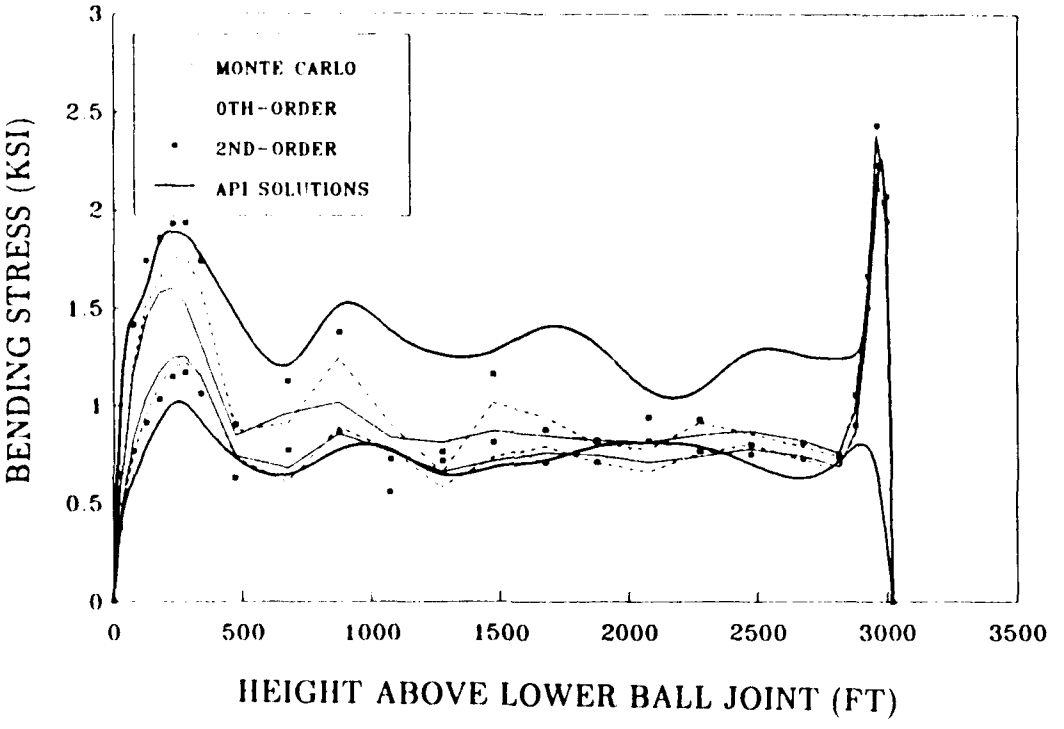

Figure 20: Maximum bending stress and bounds for riser with random top tension in 3000 feet of water.

were simulated using the AR(1) recursive formulation as

$$\bar{w}_m(z_i) = \mathrm{WN}(z_i) - \alpha_1 \bar{w}_m(z_{i-1}), \tag{109}$$

where $\mathrm{WN}(z_i)$ is Gaussian white noise and α_1 is the first–order autoregressive coefficient (Newton 1988). The correlation function for an AR(1) process is described by an exponentially decaying function expressed as

$$\rho[\tau] = (-\alpha_1)^{\tau} = \mathrm{e}^{-(\tau/L_c)}, \tag{110}$$

where

$$\alpha_1 = -\mathrm{e}^{-(1/L_c)}, \tag{111}$$

and L_c is the correlation distance. For this example $\rho[L_c] = \mathrm{e}^{-1}$, and L_c is arbitrarily chosen to be 75 feet. The coefficient of variation for the process representing the unit weight in the drilling mud is 0.2.

For this example the second–moment analysis requires as input the local spatial averages of the process and the covariance matrix between the local spatial averages. In order to predict the local spatial averages, the weight per unit length of the drilling mud is assumed to be a stationary process so that the local spatial averages were equal to the expected value of the entire process. In order to compute the covariances between the local spatial averages, the dimensionless variance function, which represents the ratio of the variance in the local spatial averages to the variance in the entire process, is required (see Chapter 2). The dimensionless variance function is computed analytically using Equation 5. The covariances between the local spatial averages are then computed using Equation 4.

For the Monte Carlo simulations, an AR(1) model is used to simulate 400 realizations of the mud weight per unit length. Each process is averaged over

the appropriate elements and the element averages are used in the finite element analyses.

A comparison of the zeroeth- and second–order solutions and the Monte Carlo predictions for the maximum displacement for the riser in 500 feet of water is presented in Figure 21. The maximum displacement plus one standard deviation is also shown. The zeroeth- and second–order estimates appear to be very near the Monte Carlo solution. For the most part the API solution bounds all of the probabilistic estimates including those which show the maximum displacement plus one standard deviation.

The maximum zeroeth- and second–order stresses and the stresses predicted using the Monte Carlo method are presented in Figure 22. The upper bounds for these predictions are also shown. The zeroeth- and second–order solutions with the addition of one standard deviation are slightly higher than the Monte Carlo estimates of the maximum stress plus one standard deviation. Note that these upper bounds for the maximum stress are significantly higher than maximum stress shown in the API solution.

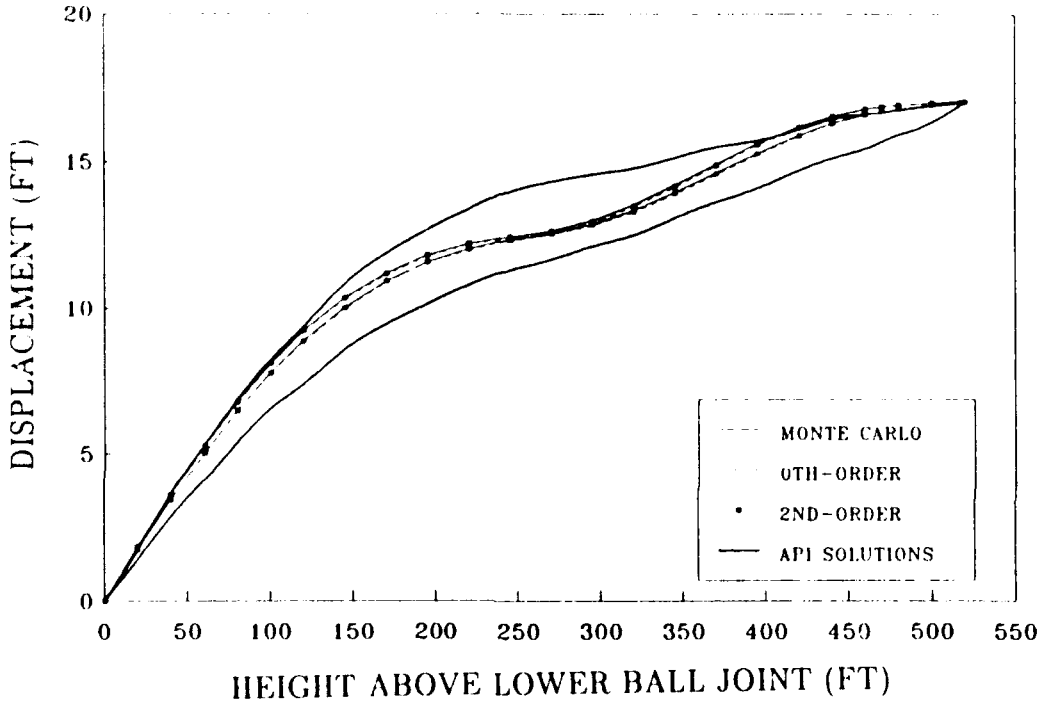

Figure 21: Maximum displacement and bounds for riser with mud weight modeled as a random field in 500 feet of water.

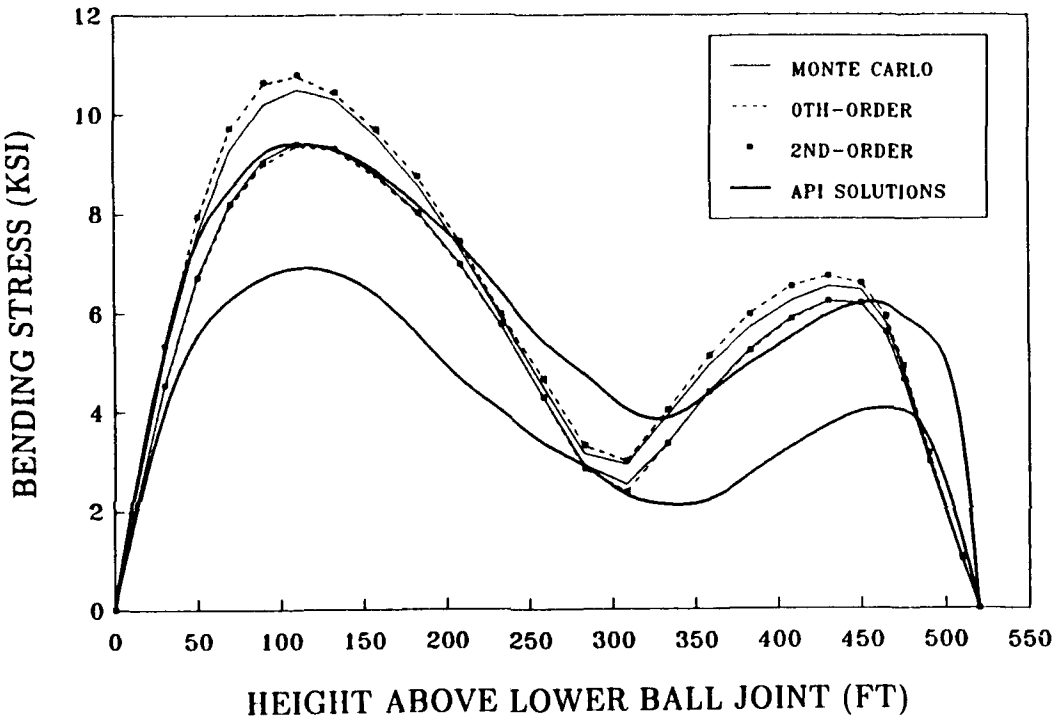

Figure 22: Maximum bending stress and bounds for riser with mud weight modeled as a random field in 500 feet of water.

5 CONCLUSIONS

The second–moment analysis method is shown to be a viable approach for estimating the probabilistic distributions in response for systems with random material properties, loads and boundary conditions. The computational aspects of the second–moment analysis method and the sequence in which they are to be implemented is shown in Figure 3. In second–moment analyses, the distributions of the sources of uncertainty are expressed in terms of their first- and second–moments, where explicit knowledge of the probability density function is not required. The correlation function must also be identified for sources of randomness which vary over the spatial coordinates.

In general, second–moment analyses are derived presuming that a linear relationship exists between the response and the sources of uncertainty. If the relationship is linear then the solutions are exact. The method may also be applied if the relationship is moderately nonlinear, provided that the coefficient of variation in the sources of uncertainty is small. If the relationship is linear then the zeroeth–order response predictions and the covariance in response obtained using the second–moment method are exact, regardless of the distributions of the sources of uncertainty. For nonlinear systems, the approximations may be improved by including higher order terms which may require that the analysis be extended beyond second–order.

Second–moment analyses require the formulation of a random vector which represents the distributions of all sources of randomness inherent to the system. The elements of the random vector correspond to the distributions of sources of randomness expressed by random variables and to the correlated distributions of the local element averages for sources of randomness expressed as random fields.

The lengths of the discrete finite elements must also be shorter than the distances over which appreciable correlation occurs in the random fields.

A simple two–degree of freedom oscillator with random spring constants was considered to demonstrate the second–moment analysis. A Monte Carlo simulation was also implemented to assess the second–moment results. The zeroeth- and second–order accurate displacements obtained using the second–moment method were compared to the displacements predicted by the Monte Carlo simulation. The zeroeth–order response solution was shown to differ from the second–order solution, where the second–order solution was almost identical to the Monte Carlo solution. The first–order accurate standard deviation predicted by the second–moment method was also compared with the standard deviation predicted by the Monte Carlo simulation. The first–order solution was shown to follow the same trend as the Monte Carlo predictions and was shown to be valid for small times, but the first–order solution overshot the Monte Carlo predictions at large times. This was a result of a resonant excitation of the higher–order terms in the second–moment analysis. For this example the advantage in the second–moment analysis as compared with the Monte Carlo method was in the computation time. The second–moment analysis required only four numerical time integrations to obtain the same responses as those predicted by the Monte Carlo method, which required 400 time integrations to obtain stable second–moment solutions.

For analyses of marine riser systems, where aspects of the problem are known to be random, the probabilistic finite element method was shown to provide useful information concerning the distributions of the response behavior. Two sets of examples were considered. In the first set of examples the tension applied to the top of the riser was modeled as a random variable. In the second set of examples the unit weight of the drilling mud contained within the riser was modeled as a

random field. For both sets of examples it was observed that while in general, the expected values of the peak second–order responses and stresses were within the ranges of estimates obtained using deterministic solutions, the addition of one standard deviation significantly impacted the response behavior. For the example riser in 500 feet of water in which the pretension was modeled as a random variable, the maximum stress shown in the API bulletin was exceeded by a factor of 1.3 when one standard deviation was added to the second–moment predictions of the maximum stress. The maximum stress predicted in the API bulletin would be exceeded by 1.7 and 2.0 times if it were to be exceeded by two and three standard deviations, respectively, of the second–moment predictions of the maximum stress. In some cases the second–order solution exceeded the bounds of conventional solutions. The riser analyses performed in this study have shown that with a small amount of variation in the tension applied at the top of the riser or with variations in the drilling mud unit weight, it can be expected that the design responses and stresses predicted using conventional finite element solutions will be exceeded.

REFERENCES

API Bulletin on Comparison of Marine Drilling Riser Analyses. (1977). API Bulletin 2J, First Edition, American Petroleum Institute, Dallas, TX.

Astill, C. J., Nossier S. B. and Shinozuka, M. (1972). "Impact Loading on Structures with Random Properties." *Journal of Structural Mechanics.* 1(1), 63–77.

Baecher, G. B. and Ingra, T. S. (1981). "Stochastic FEM in Settlement Predictions." *Journal of the Geotechnical Engineering Division.* ASCE, 107, No. GT4, 449–463.

Bathe, K. J. (1982). *Finite Element Procedures in Engineering Analysis.* Prentice–Hall, Inc. Englewood Cliffs, NJ.

Chakrabarti, S. K and Frampton, R. E. (1982). "Review of Riser Analysis Techniques." *Journal of Applied Ocean Research.* 4(102), 73–90.

Gardner, T. N. and Kotch, M. A. (1976). "Dynamic Analyses of Risers and Caissons by the Finite Element Method." *Offshore Technology Conference.* 2651, 405–420.

James, M. C., Smith G. M., Wolford J. C. and Whaley P. W. (1989). *Vibration of Mechanical and Structural Systems with Microcomputer Applications.* Harper and Row Publishers. New York, NY.

Liu, W. K., Belytschko, T. and Mani, A. (1985). "A Computational Method for the Determination of the Probabilistic Distribution of the Dynamic Response of Structures." *Computer Aided Engineering.* ASCE, 98(5), 243–248.

Liu, W. K., Belytschko, T. and Mani, A. (1986). "Probabilistic Finite Elements for Nonlinear Structural Dynamics." *Computer Methods in Applied*

Mechanics and Engineering. 56, 61–81.

Liu, W. K., Belytschko, T. and Mani, A. (1987). "Applications of Probabilistic Finite Element Methods in Elastic/Plastic Dynamics." *Journal of Engineering for Industry.* Transactions of the ASME, 109, 2–8.

Liu, W. K., Besterfield, G. and Belytschko, T. (1988a). "Transient Probabilistic Systems." *Computer Methods in Applied Mechanics and Engineering.* 67, 27–54.

Liu, W. K., Besterfield, G. and Belytschko, T. (1988b). "Variational Approach to Probabilistic Finite Elements." *Journal of Engineering Mechanics.* ASCE, 114(12), 2115–2113.

Ma, F. (1987). "Extension of Second Moment Analysis to Vector–Valued and Matrix–Valued Functions." *International Journal of Non–Linear Mechanics.* Vol. 22, No.3, 251–260.

McCoy, G. L. (1985). *Riser Response to Directional Seas.* M.S. Thesis, Department of Civil Engineering, Texas A&M University.

Newmark, N. M. (1959). "A Method of Computation for Structural Dynamics." *Journal of Engineering Mechanics Division.* ASCE, 85, 67–94.

Newton, H. J. (1988). *Timeslab: A Time Series Analysis Laboratory.* Wadsworth & Brooks/Cole Publishing Company, Pacific Grove, CA.

Niedzwecki, J. M. and Leder H. V. (1990) "Impact of Drag Force Approximations on Spectral Wave Force Predictions." Technical note submitted to *Journal of Waterway, Port, Coastal and Ocean Engineering Division.* ASCE.

Nigam, N. C. (1983). *Introduction to Random Vibrations.* The MIT Press. Cambridge, MA.

Sandt, E. W. and Niedzwecki, J. M. (1990). "Response of Flexible Structures in Random Seas." To appear in *Engineering Structures.*

Shinozuka, M. and Dasgupta, G. (1986). "Stochastic Finite Element Methods in Dynamics." *Proc. of 3rd Conf. on Dynamic Response of Structures.* Los Angeles, CA, 44–54.

Shinozuka, M. and Deodatis, D. (1988). "Response Variability of Stochastic Finite Element Systems." *Journal of Engineering Mechanics.* ASCE, 114(3), 499–515.

Vanmarcke, E. H. (1983). *Random Fields: Analysis and Synthesis.* The Massachusetts Institute of Technology Press. Cambridge, MA, and London, England.

Vanmarcke, E. H. (1984). "Stochastic Finite Element Analysis." *Probabilistic Mechanics and Structural Reliability, 4th ASCE Specialty Conference*, ed. Y. K. Wen. Berkley, CA, 278–294.

Vanmarcke, E. H. and Grigoriu, M. (1983). "Stochastic Finite Element Analysis of Simple Beams." *Journal of Engineering Mechanics.* ASCE, 109(5), 1203–1214.

Yamazaki, F., Shinozuka, M. and Dasgupta, G. (1986). "Neumann Expansion for Stochastic Finite Element Analysis." *Journal of Engineering Mechanics.* ASCE, 114(8), 1335–1354.

VITA

H. Vern Leder was born in Chicago, Illinois, on June 23, 1966. He spent most of his childhood in Hurst, Texas, where he graduated from L.D. Bell High School in 1984. In 1984, Vern entered the Ocean Engineering Program at Texas A&M University where he received his B.S. degree in May, 1988. Vern then entered the graduate college at Texas A&M in the Ocean Engineering Program. In graduate school he was employed as a Teaching Assistant and as a Research Assistant. Vern can be reached through his parents at:

429 Chisolm Trail

Hurst, Texas 76054